Quaternary Geochronology 85 (2024) 101628

Contents lists available at ScienceDirect

Quaternary Geochronology

journal homepage: www.elsevier.com/locate/quageo

# Isothermal thermoluminescence dating of speleothem growth – A case study from Bleßberg cave 2, Germany

Junjie Zhang [a,*], Jennifer Klose [b], Denis Scholz [b], Norbert Marwan [c], Sebastian F.M. Breitenbach [d], Lutz Katzschmann [e], Dennis Kraemer [f], Sumiko Tsukamoto [a,g]

[a] Leibniz Institute for Applied Geophysics (LIAG), 30655, Hannover, Germany
[b] Institute for Geosciences, University of Mainz, 55128, Mainz, Germany
[c] Potsdam Institute for Climate Impact Research (PIK), Member of the Leibniz Association, 14473, Potsdam, Germany
[d] Department of Geography and Environmental Sciences, Northumbria University, Newcastle, UK
[e] Thuringian State Office for the Environment, Mining and Nature Conservation (TLUBN), 07745, Jena, Germany
[f] Federal Institute for Geosciences and Natural Resources (BGR), 30655, Hannover, Germany
[g] Department of Geosciences, University of Tübingen, 72074, Tübingen, Germany

ARTICLE INFO

*Keywords:*
Speleothem
Calcite
Isothermal thermoluminescence dating
Th/U dating

ABSTRACT

Speleothems are a key archive of past climatic and environmental changes. $^{230}$Th/U dating is the most commonly used method to determine speleothem ages. However, incorporation of non-radiogenic thorium may hamper $^{230}$Th/U dating, and samples older than 600 ka also remain out-of-reach. Calcite exhibits a thermoluminescence (TL) signal at 280 °C with a high characteristic saturation dose, and provides significant potential to date carbonate samples over several million years. Hitherto, the application of TL dating for calcite has mainly been hindered by two factors: 1) a spurious TL signal occurring in the high temperature range, and 2) non-uniform dose rate due to U-series disequilibrium. Here we test an isothermal TL (ITL) dating method on a speleothem sample from Bleßberg cave 2, Germany. We show that the ITL signal measured at 240 °C can completely remove the 280 °C TL peak with a negligible TL contribution from the higher temperature range, thus reducing the influence from the spurious signal. The time-dependent dose rate variation can be simulated using the initial radioactivity of $^{238}$U, $^{234}$U, $^{230}$Th and their decay constants. We use the $^{230}$Th/U dating method to provide precise and accurate radiometric ages documenting that the speleothem grew between 425.5 ± 5.4 and 320.5 ± 9.7 ka. The ITL ages (421 ± 23 to 311 ± 23 ka) of four subsamples from the speleothem are consistent with the $^{230}$Th/U ages at isochronous sampling positions, showing the general reliability of the ITL dating method. ITL dating provides a pathway to construct chronologies for palaeoclimate reconstructions for speleothems beyond the range of the $^{230}$Th/U-method and for samples that are unsuitable for U-series dating methods.

## 1. Introduction

Speleothems are secondary carbonate precipitated from dripwater in caves mostly in limestone or dolomite bedrock (Moore, 1952). The wide distribution of speleothems and their exceptional suitability for high accuracy and precision $^{230}$Th/U dating make them extraordinary terrestrial archives of past climatic and environmental changes (Henderson, 2006; Scholz and Hoffmann, 2008; Cheng et al., 2016). However, $^{230}$Th/U dating has an upper limit of approximately 600 ka (Scholz and Hoffmann, 2008; Cheng et al., 2016), and it is not applicable for samples older than 600 ka and for samples with incorporation of non-radiogenic thorium. U-Pb dating is also applicable for speleothem samples with hundreds of millions of years in ages (Richards et al., 1998; Woodhead et al., 2006; Pickering et al., 2010; Woodhead and Petrus, 2019). However, U-Pb requires samples with high U and low common Pb, and the majority of speleothem samples is not suitable for U-Pb dating.

Thermoluminescence (TL) dating has been performed on calcite from various geological backgrounds, such as speleothem, limestone, calcite vein, and biogenic carbonate (Wintle, 1975, 1978; Aitken and Wintle, 1977; Aitken and Bussell, 1982; Debenham, 1983; Franklin et al., 1988; Ninagawa et al., 1992, 1994; Engin and Güven, 1997; Duller et al., 2009; Yee and Mo, 2018). TL dating measures the irradiation dose the calcite has received since its crystallisation. Dividing the received dose by the

* Corresponding author.
*E-mail address:* junjie.zhang@leibniz-liag.de (J. Zhang).

https://doi.org/10.1016/j.quageo.2024.101628
Received 21 May 2024; Received in revised form 16 September 2024; Accepted 17 September 2024
Available online 21 September 2024

environmental dose rate, the crystallisation age can be obtained. The characteristic TL peak at ~280 °C (with a heating rate of 5 °C/s) is mostly applied for dating calcite. Despite the low precision of TL dating compared to the $^{230}$Th/U dating method, TL dating has the potential to date samples up to tens of millions of years because of the high saturation dose ($D_0$ up to 5000 Gy) of the TL signal (Wintle, 1978; Debenham, 1983; Debenham and Aitken, 1984; Duller et al., 2009; Stirling et al., 2012; Zhang and Wang, 2020). However, several drawbacks of TL dating with calcite have hindered its application. One obstacle is the existence of a spurious TL signal at the high temperature range (Wintle, 1975; Bangert and Hennig, 1979; Pagonis et al., 1997). The spurious TL signal is not related to radiation, and its existence will result in overestimation of the equivalent dose ($D_e$). Some studies suggested that the spurious TL signal was caused by the mechanic damage of the grain surface during the pretreatment of the calcite sample, such as grinding, and applying acetic etching to remove the surface layer of the calcite grains indeed helped to suppress the spurious signal (Wintle, 1975, 1978; Ninagawa et al., 1988). However, in some studies, the etching treatment failed to remove the spurious TL signal completely (Bangert and Hennig, 1979; Pagonis et al., 1997), and other hypotheses have been proposed for the origin of the spurious TL signal, such as the presence of trapped organic matter (Bangert and Hennig, 1979; Rogue et al., 2001; Liao et al., 2014), oxygen absorption and desorption (Bangert and Hennig, 1979) and carbonate decomposition during heating (Rogue et al., 2001). It has also been reported that after being removed by heating, the spurious TL signal can still be regenerated after several days of storage (Pagonis et al., 1997). Another drawback for TL dating of calcite is that the multiple-aliquot additive-dose protocol (MAAD) is usually needed for $D_e$ measurements (Wintle, 1978; Debenham, 1983; Debenham and Aitken, 1984; Yee and Mo, 2018), as heating to a high temperature (e.g., 400 °C) will change the luminescence sensitivity significantly. The MAAD protocol consumes large amounts of sample, and has a larger error in $D_e$ estimation. Moreover, as the MAAD applies extrapolation to calculate the $D_e$, it will bring in large uncertainty for very old samples (e.g., $D_e > 5000$ Gy).

Another major challenge in TL dating of calcite is the complexity of dose rate evaluation. The dose rate fluctuates over time due to the disequilibrium in the U decay chain since the crystallisation of calcite (Wintle, 1978; Ikeya and Ohmura, 1983). Furthermore, the alpha irradiation will dominate the total dose rate of calcite samples, making the alpha efficiency value ($a$-value) a critical parameter. However, the reported $a$-values can vary significantly between samples (e.g., Wintle, 1978; Debenham and Aitken, 1984).

Instead of heating the aliquots to a high temperature (e.g., 400 °C) to obtain the 280 °C TL peak, the aliquots can be kept at a relatively lower temperature (e.g., 240 °C) for long time to measure an isothermal TL (ITL) signal which is equivalent to the 280 °C TL peak. The ITL dating protocol has been widely applied for quartz (Murray and Wintle, 2000; Buylaert et al., 2006; Choi et al., 2006; Tsukamoto et al., 2007; Vandenberghe et al., 2009; Tang and Li, 2015; Rahimzadeh et al., 2023). As the ITL signals are measured at relatively lower temperatures, the luminescence sensitivity change is smaller and the single-aliquot regenerative-dose (SAR) protocol can be applied, which improves the accuracy and precision of $D_e$ estimation compared to the MAAD protocol used for TL dating. Recent studies applied ITL measurements at 235 or 240 °C on calcite samples, and reported that the ITL SAR protocol has the potential to measure $D_e$ accurately with negligible influence from the spurious signal (Zhang and Wang, 2020; Huang et al., 2022). Hitherto, the reliability of the ITL SAR protocol in dating calcite has not been tested on samples with independent age control.

In this study, we test the ITL SAR protocol on a speleothem sample from Bleßberg cave 2, Germany. $^{230}$Th/U dating is performed on this speleothem sample which provides precise independent age control. The characteristics of the ITL signal and the 280 °C TL peak, such as the signal stability, saturation dose and bleachability, are studied. We apply both the ITL SAR and TL MAAD protocols and compare their performance on $D_e$ measurements. To calculate the dose rate, we accurately measure the alpha efficiency and calculate the annual dose year by year based on the initial radioactivity of $^{238}$U, $^{234}$U, $^{230}$Th and their decay constants. Finally, we compare the ITL ages with the $^{230}$Th/U ages to discuss the reliability of ITL dating.

## 2. Sample details

The Bleßberg cave and Bleßberg cave 2 (also called Herrenberg cave and Herrenberg cave 2) (Rusznyák et al., 2012) are located in Thuringia, Germany (50°25′28″ N, 11°01′13″ E) (Fig. S1). The Bleßberg cave was discovered in March, Bleßberg cave 2 in May 2008 during the construction of a tunnel for a new railway line. The sample used in this study is from cave 2. The much smaller cave 2 is located only 60 m ahead of the tunnel portal and has a height till over 4 m, a width of 2–4 m and an explored length of around 90 m. The cave 2 is overlain by about 10 m thickness of Triassic marly limestone (Lower Muschelkalk/Anisium). The bed is partly formed by several meter thick, relatively young debris and lies well above the active karst level. Inside the cave, active dripping points and speleothems can only be found to a limited extent. Older speleothems, mostly in the form of flowstones and draperies, on up to two floors characterize sections of the western part of the cave (Wunderlich et al., 2009). The cave had, like the larger Bleßberg cave (Breitenbach et al., 2019), no natural entrances before the discovery in 2008, and had not been disturbed by animal or human activities, providing an ideal place for paleoclimate and palaeoenvironmental reconstructions. A heart shaped flowstone drapery (sample BB2-1) was collected from the wall of the cave in 2009 (Fig. S1). The sample was cut into slices to reveal the growth bandings. Slices were prepared for different analyses, such as trace element mapping, carbon and oxygen isotope analysis, $^{230}$Th/U dating and ITL dating. The slice used for ITL dating is shown on Fig. 1.

## 3. Petrologic study and trace element mapping

Four subsamples were collected from one slice of BB2-1 (the same slice used for ITL dating), to perform X-ray diffraction (XRD) analyses with a PANalytical MPD Pro XRD equipment at the Federal Institute for Geosciences and Natural Resources (BGR), Hannover, Germany. Results show that the speleothem sample is pure calcite (Fig. S2). Two thin sections were prepared and observed under a petrographic microscope. The sample is compact and the grain sizes of the calcite crystals vary significantly at different positions, ranging from <100 μm to larger than 500 μm (Fig. S3).

Micro-energy dispersive X-ray fluorescence (μ-EDXRF) can generate 2D element distribution images that provide textural and spatially resolved chemical information (Rammlmair et al., 2006). One slice of the speleothem was polished on the surface, and used for μ-EDXRF analysis at BGR. The X-ray was excited with an Rh tube with 50 kV and 600 μA. The beam diameter was 18 μm, and the element distribution images were recorded at a measuring distance of 40 μm with a measuring time of 1 ms per measuring point. The growth layers are clearly visible from the element distribution, and two major growth phases can be identified by their different element concentrations (Fig. 1B).

## 4. $^{230}$Th/U dating

$^{230}$Th/U dating was conducted at the Institute for Geosciences, Johannes Gutenberg University (JGU) Mainz. In total, fourteen $^{230}$Th/U-ages were determined. Approximately 50 mg of sample material was drilled using a handheld drill and processed in a clean laboratory to

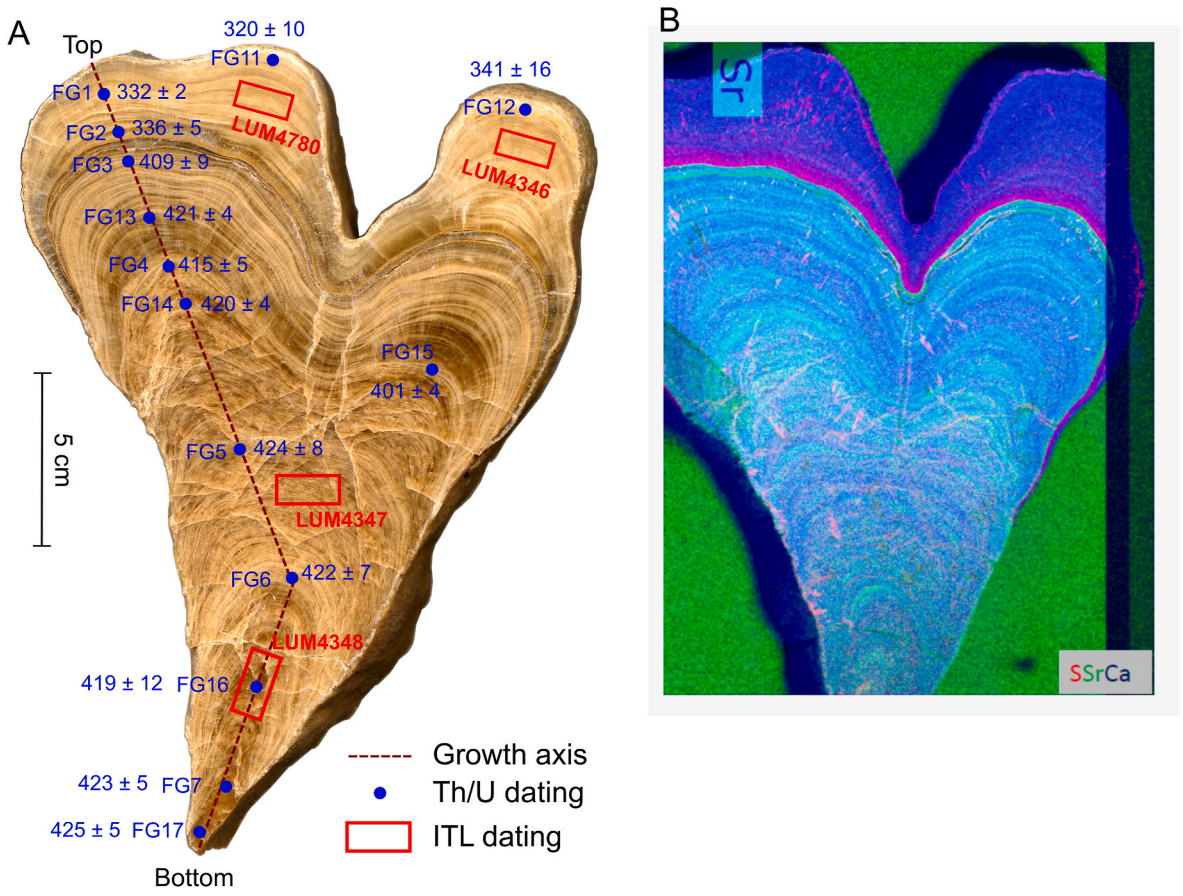


**Fig. 1.** The speleothem sample (BB2-1) used in this study. A) Sampling positions for $^{230}$Th/U dating and ITL dating. The numbers in blue represent rounded $^{230}$Th/U ages in ka. B) Elements distribution revealed by μ-EDXRF analysis. The intensities of the red, green and blue colours indicate the elemental abundance of S, Sr, and Ca, respectively. The green rectangle in the top-left resembles a piece of Sr standard.(For interpretation of the references to colour in this figure legend, the reader is referred to the web version of this article.)

separate U and Th. The samples were weighed, dissolved in 7N $HNO_3$ and subsequently spiked with a previously calibrated $^{229}$Th-$^{233}$U–$^{236}$U spike solution. The samples were dried down, treated with concentrated $HNO_3$, HCl and $H_2O_2$ to destroy potential organic material and then again evaporated and dissolved in 7N $HNO_3$. The samples were further passed through ion exchange columns filled with 1.5 mL of Bio-Rad AG 1-X8 (200–400 mesh size) anion exchange resin following the procedure described in Yang et al. (2015). Mass spectrometric analyses of U and Th were conducted using a Thermo Fisher Neptune Plus multi-collector inductively coupled plasma mass spectrometer (MC-ICP-MS) equipped with an Elemental Scientific Apex Omega HF desolvator. U and Th were measured separately in a standard-bracketing procedure, and the data were corrected offline using an in-house code written in R (R Core Team, 2022). All activity ratios and ages were calculated using the decay constants of Cheng et al. (2013). To account for potential detrital contamination, the ages were corrected assuming an upper continental crust $^{232}$Th/$^{238}$U weight ratio of 3.8 ± 1.9 (Wedepohl, 1995) and secular equilibrium between $^{230}$Th, $^{234}$U, and $^{238}$U. Details of the measurements can be found in Obert et al. (2016). The Th/U results are summarised in Table 1. Ten Th/U ages are from Marine Isotope Stage (MIS) 11 and four

**Table 1**
Results of the$^{230}$Th/U-dating. Activity ratios are indicated within parentheses. $[^{234}U/^{238}U]_0$ is the initial activity ratio of $^{234}$U and $^{238}$U when the speleothem crystallised. Age errors are 2σ.

| Sample ID | $^{238}$U (ppm) | $^{232}$Th (ppb) | $[^{234}U/^{238}U]$ | $[^{230}Th/^{238}U]$ | $[^{234}U/^{238}U]_0$ | $Age_{uncorrected}$ (ka) | $Age_{corrected}$ (ka) |
|---|---|---|---|---|---|---|---|
| FG1 | 0.5325 ± 0.0036 | 5.134 ± 0.035 | 1.6035 ± 0.0009 | 1.7178 ± 0.0020 | 2.54 ± 0.01 | 331.77 ± 1.76 | 331.66 ± 2.06 |
| FG2 | 0.2815 ± 0.0021 | 8.272 ± 0.062 | 1.8593 ± 0.0034 | 2.0487 ± 0.0049 | 3.22 ± 0.03 | 336.47 ± 2.26 | 336.22 ± 4.74 |
| FG3 | 0.5658 ± 0.0034 | 22.45 ± 0.137 | 1.4975 ± 0.0026 | 1.6415 ± 0.0038 | 2.58 ± 0.04 | 409.33 ± 3.61 | 408.90 ± 9.07 |
| FG4 | 0.8743 ± 0.0075 | 5.677 ± 0.049 | 1.5180 ± 0.0007 | 1.6723 ± 0.0023 | 2.67 ± 0.02 | 415.13 ± 4.26 | 415.06 ± 4.61 |
| FG5 | 0.8868 ± 0.0057 | 24.83 ± 0.160 | 1.5283 ± 0.0020 | 1.6911 ± 0.0030 | 2.75 ± 0.03 | 424.61 ± 3.38 | 424.32 ± 7.69 |
| FG6 | 0.8312 ± 0.0060 | 21.85 ± 0.158 | 1.5318 ± 0.0018 | 1.6947 ± 0.0029 | 2.75 ± 0.03 | 422.27 ± 3.48 | 422.00 ± 7.28 |
| FG7 | 0.9150 ± 0.0057 | 12.12 ± 0.075 | 1.5521 ± 0.0011 | 1.7224 ± 0.0021 | 2.82 ± 0.02 | 423.00 ± 3.46 | 422.87 ± 4.76 |
| FG11 | 0.3875 ± 0.0023 | 35.36 ± 0.213 | 1.5195 ± 0.0062 | 1.5994 ± 0.0074 | 2.28 ± 0.03 | 321.61 ± 1.97 | 320.49 ± 9.73 |
| FG12 | 0.4120 ± 0.0026 | 53.11 ± 0.341 | 1.5240 ± 0.0089 | 1.6265 ± 0.0108 | 2.37 ± 0.05 | 342.86 ± 2.34 | 341.31 ± 16.12 |
| FG13 | 0.5553 ± 0.0032 | 3.934 ± 0.022 | 1.5393 ± 0.0007 | 1.7042 ± 0.0019 | 2.77 ± 0.02 | 421.07 ± 3.56 | 421.00 ± 4.00 |
| FG14 | 0.8164 ± 0.0056 | 5.195 ± 0.036 | 1.5294 ± 0.0007 | 1.6903 ± 0.0019 | 2.73 ± 0.02 | 419.95 ± 3.68 | 419.88 ± 4.03 |
| FG15 | 0.6938 ± 0.0062 | 2.487 ± 0.022 | 1.5161 ± 0.0006 | 1.6615 ± 0.0020 | 2.60 ± 0.02 | 400.76 ± 3.40 | 400.72 ± 3.56 |
| FG16 | 0.8940 ± 0.0053 | 41.30 ± 0.244 | 1.5572 ± 0.0033 | 1.7273 ± 0.0047 | 2.82 ± 0.05 | 419.72 ± 3.54 | 419.26 ± 11.66 |
| FG17 | 0.8187 ± 0.0048 | 12.35 ± 0.072 | 1.5584 ± 0.0012 | 1.7323 ± 0.0023 | 2.86 ± 0.03 | 425.60 ± 3.87 | 425.46 ± 5.42 |

ages are from MIS 9.

## 5. Luminescence dating

### 5.1. Sample preparation and instrumentation

Sample preparation and luminescence measurements for $D_e$ values were performed at the Leibniz Institute for Applied Geophysics (LIAG), Hannover. Four subsamples (LUM4346, 4347, 4348, 4780) were cut with a saw from the center, middle and outer rim of one slice of speleothem BB2-1 (Fig. 1). Sample preparation was performed under subdued red light. The surface of the subsamples was etched with 10 % hydrochloric (HCl) acid to avoid effects of light exposure because previous studies have shown that natural daylight can deplete the TL signal of calcite (Liritzis, 1994; Liritzis and Bakopoulos, 1997). The subsamples weighed 4.3–5.6 g. The volume of the 10 % HCl acid was calculated (~20 mL) for each subsample to dissolve ~50 % weight of the subsample. The reaction generally finished within 30 min. The remaining pieces were washed by distilled water, gently crushed under water in an agate mortar and wet sieved to separate grains with a size of 100–200 μm. To avoid the generation of spurious signals, the crushing was only applied for ~1 min and grinding was avoided (Wintle, 1975). These 100–200 μm grains were mounted on stainless steel discs, to prepare the aliquots (6 mm diameter) for luminescence measurements. Measurements were performed on a Risø TL/OSL DA-15 reader. $A^{90}Sr/^{90}Y$ beta source is mounted inside the reader. Its beta dose rate was calibrated to be 0.12 Gy/s using the coarse-grain Risø calibration quartz, which had received a gamma irradiation of 4.81 Gy. Considering the similar beta stopping powers and the gamma absorption coefficients between quartz and calcite minerals (from Table 5.1 of Aitken, 1985), the beta source dose rate for calcite was also 0.12 Gy/s. The TL glow curves and the ITL signals were measured in an $N_2$ atmosphere. Heating rates were 5 °C/s if not specified otherwise. Previous studies found that the TL emission of calcite peaked at ~550 nm (McDougall, 1968; Wintle, 1978). The signals were detected by an EMI 9235QB photomultiplier tube through a single 2 mm thick Schott BG-39 filter (transmission band of 300–700 nm).

### 5.2. Equivalent dose measurements

#### 5.2.1. MAAD protocol

The MAAD protocol was tested with the TL peak signal at 280 °C (details in Table 2). Weights of aliquots were measured for mass normalisation (Debenham and Aitken, 1984; Wintle, 1978). Meanwhile, two kinds of low-temperature TL peak normalisation methods were tested for LUM4347. The aliquots were firstly given a small test dose (5 Gy), followed by heating to 200 °C to measure the corresponding low-temperature TL peak at ca. 100 °C ($T_1$). The aliquots were then divided into several groups, given different additive doses (from 0 to 600 Gy). Aliquots were heated to 250 °C to remove the unstable low-temperature TL signal. Small test doses (5 Gy) were then administered again. TL glow curves were measured at up to 400 °C with background subtraction. In this step, the glow curve contains the 280 °C TL peak ($L_x$) corresponding to the natural plus additive dose and the 100 °C TL peak corresponding to the small dose ($T_2$) (Fig. 2). The $T_1$ and $T_2$ signals were integrated from 80 to 120 °C, and the $L_x$ signals from 270 to 290 °C.

The $T_1$ represents the TL response to a fixed dose, which can represent the mass of the aliquot (Zhang and Tsukamoto, 2022). The $T_2$ normalisation is also called the zero glow monitoring (ZGM) technique (Aitken and Bussell, 1979; Duller et al., 2009). An advantage of the ZGM normalisation is that the 280 °C TL peak used for dating and the 100 °C TL peak used for normalisation can be shown in the same glow curve (Fig. 2A). $D_e$ was estimated with three different normalisation methods: mass normalisation, $T_1$ normalisation and $T_2$ normalisation (Fig. 2B–D). The two small test doses (a total of 10 Gy) were added to the additive doses when estimating the $D_e$ values. The $D_e$ results are 245 ± 27 Gy and 244 ± 28 Gy with mass normalisation and $T_1$ normalisation, respectively, which are identical to each other. However, the $T_2$ normalisation gives a higher $D_e$ of 308 ± 35 Gy. Mass normalised $T_1$ is independent of the additive doses while mass normalised $T_2$ increases with larger additive doses, as the $T_2$ signal is measured after the additive dose administration (Fig. 3A). Such kind of 'pre-dose effect' on $T_2$ results in an underestimated slope on the $L_x/T_2$ vs. dose plot, and consequently an overestimated $D_e$. As the $T_1$ signal is measured before any treatments with all aliquots in their initial states, the $T_1$ normalisation is equivalent to mass normalisation in $D_e$ estimation. However, $T_1$ normalisation is a more practical method as weighing aliquots is laborious and may risk grain loss between weighing and luminescence measurement.

The *plateau test* is commonly used in TL dating to identify the stable region of the TL glow curve (Aitken, 1985). With $T_1$ normalisation, MAAD $D_e$ values were estimated with TL signals at different temperature intervals ($T$ ± 10 °C, $T$ from 230 to 320) for LUM4347. A $D_e$ plateau is reached when $T$ is between 270 and 285 °C (Fig. 3B). The smaller $D_e$ values in the temperature range lower than 270 °C indicate TL signals below 270 °C are not thermally stable. Whereas, the larger $D_e$ values in the higher temperature range (>285 °C) are likely a result of contamination of the spurious TL signal. In this study, the samples underwent only mild crushing. Consequently, the impact of spurious TL signals on the 280 °C TL peak is minimal, allowing us to maintain a $D_e$ plateau within the 270–285 °C range. MAAD $D_e$ values were also measured for other subsamples with the $T_1$ normalisation method (Table 3).

#### 5.2.2. SAR protocol

The net TL loss removed by ITL measurements at 240 °C ($ITL_{240}$) over 200 s is shown in Fig. 4A. The $ITL_{240}$ signal can perfectly isolate the 280 °C TL peak with negligible contribution from the higher temperature range. Net TL loss by ITL measurements at other temperatures are also shown in Fig. 4B. The SAR dating protocol with the ITL measurement is shown in Table 2. It is adapted from Zhang and Wang (2020) with small modifications. The duration of ITL measurement was reduced from 500 s to 200 s, and the cleaning step at the end of each cycle (heated to 400 °C) in Zhang and Wang (2020) was also removed, as the $ITL_{240}$ measurement for 200 s can completely remove the 280 °C TL peak (Fig. 4A). The $ITL_{240}$ curves of the natural signal and different regenerative doses from one aliquot of LUM4346 are shown on Fig. 5A. The ITL signals increased in the first 5 s because of the thermal lag between the heating plate and the disc, thus the 6–15 s signal was integrated for $D_e$ estimation with the last 181–200 s signal subtracted as background. Increasing the length of the integration period has negligible influence on the $D_e$ values (Fig. S4). The dose-response curve (DRC) of the $ITL_{240}$ signal can be well fitted with a single saturating exponential function, and the recycling ratio is very close to unity indicating successful sensitivity correction (Fig. 5B). For the four subsamples, 6–12 aliquots were measured for each, and the

**Table 2**
The MAAD protocol for $D_e$ measurement with TL signal, and the SAR protocol for $ITL_{240}$ signal.

| MAAD | | | SAR | | |
|---|---|---|---|---|---|
| Step | Treatments | Signal | Step | Treatments | Signal |
| 1 | Give a small test dose (5 Gy) | | 1 | Regeneration dose ($D_i$, 0 Gy for the first cycle) | |
| 2 | Heat to 200 °C | $T_1$ | 2 | Heat to 250 °C | |
| 3 | Give additive dose, for different groups of aliquots | | 3 | Isothermal TL at 240 °C for 200s | $L_x$ |
| 4 | Preheat to 250 °C | | 4 | Test dose | |
| 5 | Give a small test dose (5 Gy) | | 5 | Heat to 250 °C | |
| 6 | TL to 400 °C with BG subtraction | $T_2$, $L_x$ | 6 | Isothermal TL at 240 °C for 200s | $T_x$ |
| | | | 7 | Return to step 1 | |

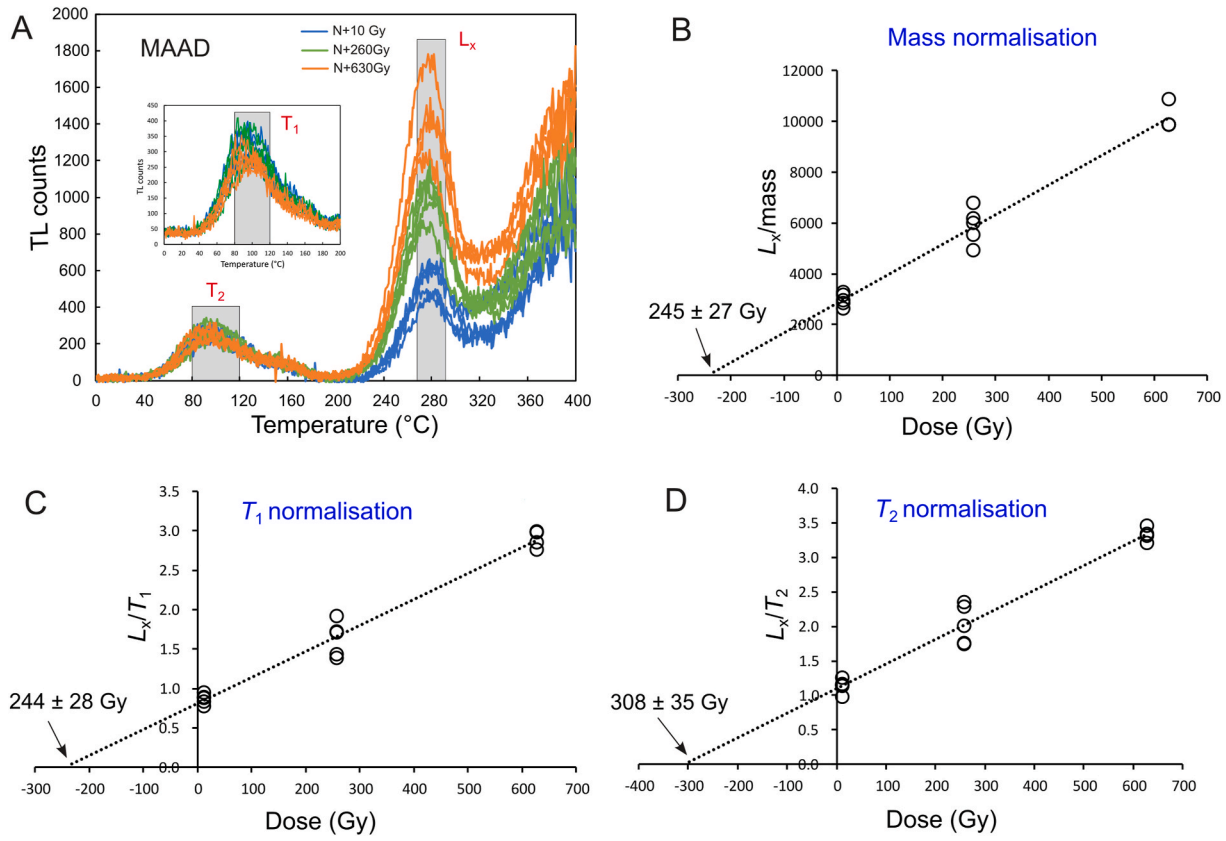


**Fig. 2.** MAAD $D_e$ estimation for the 280 °C TL peak of LUM4347. A) TL curves of aliquots with different additive doses. The low-temperature TL peak at ~100 °C corresponds to a small dose (5 Gy). $D_e$ estimation with B) mass normalisation, C) $T_1$ normalisation, D) $T_2$ normalisation.

mean $D_e$ values were used for age determination. The test dose was generally 50 % of the $D_e$ for each subsample. To obtain a better constraint for the characteristic saturation dose ($D_0$) of the $ITL_{240}$ signal, one aliquot of LUM4346 was given high regenerative doses up to 12000 Gy (with a test dose of 360 Gy), and the $D_0$ is 4975 ± 818 Gy (inset plot in Fig. 5B).

SAR $D_e$ values were measured at different ITL temperatures for sample LUM4346, with 4–8 aliquots for each temperature. The SAR $D_e$ values reach a plateau at the ITL temperature range between 230 and 240 °C (Fig. 5C). The smaller ITL $D_e$ values below 230 °C should be related to lower thermal stability, whereas the larger ITL $D_e$ values above 240 °C are likely due to the influence of the spurious signal. However, ITL $D_e$ values of sample LUM4347 are more scattered and they are roughly close to each other at the temperature range of 230–255 °C. $D_e$ values of the $ITL_{240}$ signal are applied for age estimation for all subsamples (Table 3).

Dose recovery tests were performed on LUM4346 with a single aliquot regenerative additive dose (SARA) protocol (Mejdahl and Bøtter-Jensen, 1994). Three groups of aliquots (7 aliquots in each group) were given doses of 0, 175, and 350 Gy on top of the natural dose. The aliquots were then measured with the same $ITL_{240}$ SAR protocol as used for $D_e$ measurement. The recovered doses were plotted against the additive doses in Fig. 5D. The dose recovery ratio (DRR) is 0.93 ± 0.11, indicating the reliability of $D_e$ measurements with the ITL SAR protocol.

### 5.3. Luminescence characteristics

#### 5.3.1. Thermal stability

Low thermal stability of a luminescence signal will result in age underestimation. The peak shifting method (Hoogentraaten, 1958) was applied to obtain the trap kinetic parameters for LUM4347, LUM4348 and LUM4780, with 3–4 aliquots for each subsample. The aliquots were heated to 400 °C to remove the natural signals. A fixed regenerative dose of 360 Gy was administered to the aliquots. After being preheated to 250 °C (5 °C/s), the TL signals were measured up to 400 °C (with background subtraction) at various heating rates of 1.6, 0.8, 0.4, 0.2, and 0.1 °C/s. The peak shifted to a lower temperature with a lower heating rate (Fig. 6A). Heating rates used here are relatively low to minimise the thermal lag between the heating plate and the steel disc. The deduced trap depth ($E$) and the frequency factor ($s$) are quite close to each other between different aliquots and different subsamples (Table S1). The arithmetic mean $E$ and the geometric mean $s$ of all aliquots are 1.78 eV and 1.24 × $10^{16}$ $s^{-1}$. The current air temperature inside the Bleßberg cave is 8.7 ± 0.1 °C (Breitenbach et al., 2019). Cave air temperature reflects the mean annual surface atmosphere temperature (Wigley and Brown, 1976; Domínguez-Villar et al., 2013). The average air temperature inside the Bleßberg cave over the last several glacial-interglacial cycles should be smaller than the present cave air temperature as it is now in a warm period. Thermal lifetime of the luminescence signal increases with lower temperature. To make more conservative estimation, we assumed an average temperature of 10 °C, and calculated the corresponded lifetimes ($\tau_{10}$). The $\tau_{10}$ of the 280 °C TL peak from the mean $E$ and $s$ is 109 Ma.

The same aliquots of LUM4347 and LUM4780 that were used for peak shifting were also applied for isothermal annealing tests to measure the $E$ and $s$ values of the $ITL_{240}$ signal. The given dose was fixed to 120 Gy for all aliquots. After being preheated to 250 °C (5 °C/s), the aliquots were heated at different temperatures (180, 200, 220, and 240 °C) for different periods (1, 10, 20, 40, 80, 160, 400, 1000, and repeatedly 40 s), and the $ITL_{240}$ was measured afterwards ($L_x$). A test dose of 120 Gy was given, and the corresponding $ITL_{240}$ signal was measured directly after being preheated to 250 °C ($T_x$). The sensitivity corrected $ITL_{240}$ signal ($L_x/T_x$) decreased with longer annealing time (Fig. 6B). The 40 s isothermal annealing was repeated twice and their $L_x/T_x$ values were

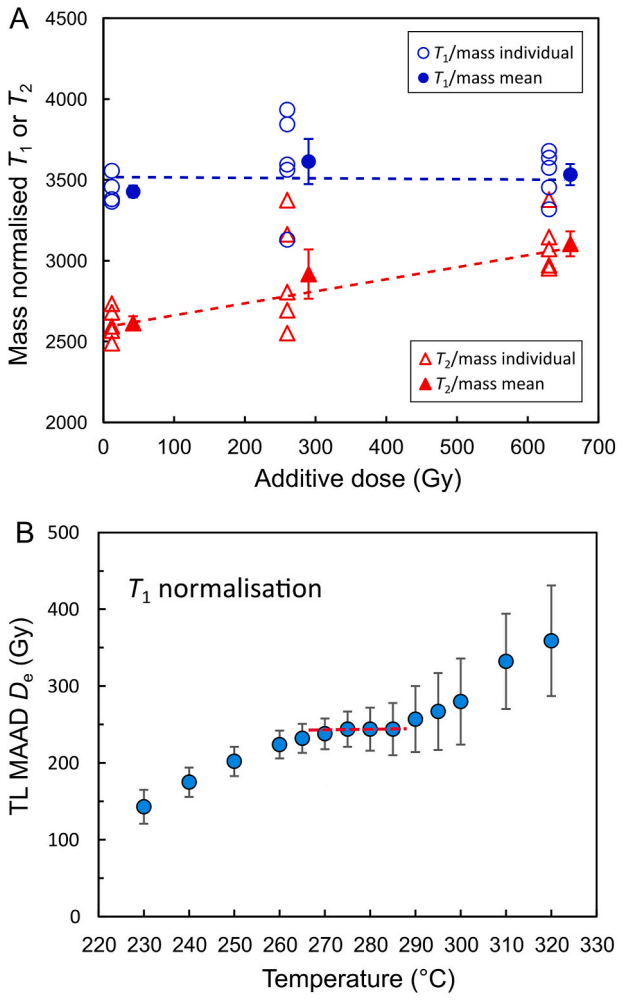


**Fig. 3.** A) Mass normalised $T_1$ and $T_2$ for LUM4347. Note that the sensitivity of $T_2$ increases with larger additive dose. B) MAAD $D_e$ values for TL signals from different temperature ranges. Note that there is a $D_e$ plateau between the temperature range between 270 and 285 °C.

compared to examine the reliability of sensitivity correction, similar to the recycling ratio. The ratios are always within 1.00 ± 0.05, indicating successful sensitivity correction. The *E* and *s* values vary substantially between aliquots and subsamples. The cause of this variation is not clear, but one possibility is the low reproducibility achievable with the used instrumentation when applying the isothermal annealing method. However, the arithmetic mean *E* and the geometric mean *s* of all aliquots are 1.80 eV and 1.84 × $10^{16}$ $s^{-1}$, which are still similar to those of the 280 °C TL peak. The $\tau_{10}$ of the $ITL_{240}$ signal from the mean *E* and *s* is 186 Ma. The similar $\tau_{10}$ values of the $ITL_{240}$ signal and the 280 °C TL peak are consistent with the fact that the $ITL_{240}$ signal is sourced from the same trap as the 280 °C TL peak. The *E* and *s* values obtained from the peak shifting method may be more accurate since the inter-aliquot variation is much smaller.

Isothermal annealing tests were also performed for the 280 °C TL peak with two aliquots from subsample LUM4347 (Fig. 6C). The isothermal annealing sequence used for 280 °C TL peak was identical to that of the $ITL_{240}$ signal, except that the $ITL_{240}$ measurements were replaced by the TL measurements up to 400 °C. The mean *E* is 1.61 eV, and the mean *s* is 1.01 × $10^{14}$, corresponding to a $\tau_{10}$ of 11 Ma. Considering the limited number of aliquots used for this method and the lower reproducibility with the isothermal annealing test, this shorter $\tau_{10}$ of 11 Ma is regarded as less reliable than the 109 Ma deduced from peak shifting method, and it will not be used in the following discussion.

The variation of lifetime with changing temperature is shown in Fig. 6D, with *E* and *s* values for the 280 °C TL peak (with the peak shifting method) and the $ITL_{240}$ signal, respectively. Lifetime is very sensitive to temperature. For example, the lifetime of the 280 °C TL peak is 109 Ma at 10 °C, but it decreases to 9.1 Ma at a higher temperature of 20 °C, and increases to 404 Ma at a lower temperature of 5 °C.

The $\tau_{10}$ values of this study are summarised in Table S1, together

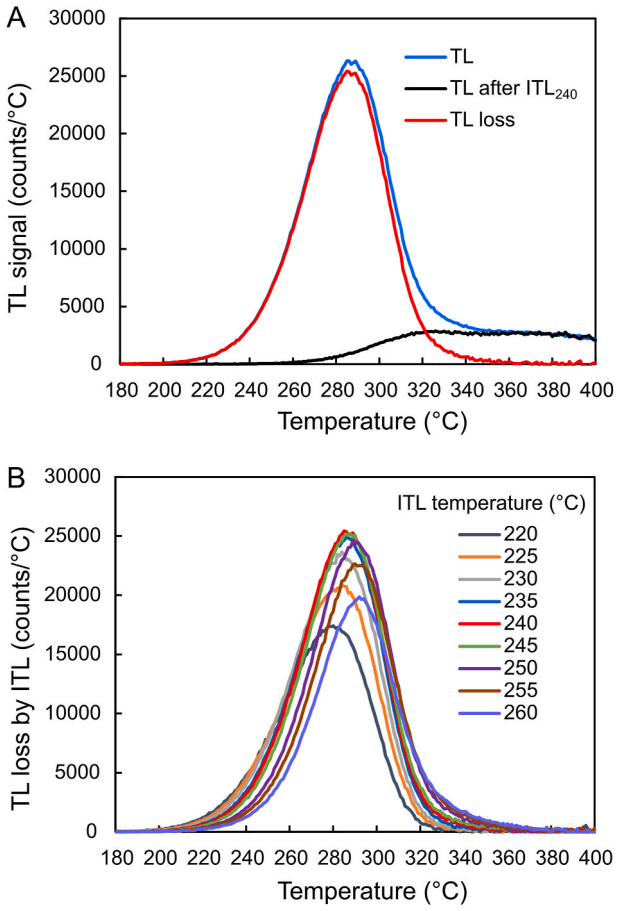


**Fig. 4.** A) TL signals before and after the ITL measurement at 240 °C ($ITL_{240}$) for 200 s on an aliquot of LUM4347, and the net TL signal removed by $ITL_{240}$ measurement. The TL signal corresponds to a regenerative dose of 120 Gy. B) Net TL signals removed by ITL signals at different temperatures on the same aliquot. Note that the preheat temperature is always 10 °C higher than the ITL temperature.

**Table 3**
Results of TL/ITL dating. U concentrations are from line scan LA-ICP-MS measurements. The simulated and iterated ITL ages are calculated based on the $ITL_{240}$ $D_e$ values. Errors of $^{230}Th/U$ ages are 2σ. Errors of ITL ages are 1σ.

| LUM ID | Th/U ID | $[^{234}U/^{238}U]_0$ | U (ppm) | $^{230}Th/U$ age (ka) | 280 °C TL $D_e$ (Gy) | $ITL_{240}$ $D_e$ (Gy) | Iterated age (ka) | Simulated age (ka) |
|---|---|---|---|---|---|---|---|---|
| LUM4780 | FG1 | 2.54 ± 0.01 | 0.42 ± 0.02 | 331.66 ± 2.06 | 109 ± 17 | 109.7 ± 7.6 | 311 ± 26 | 311 ± 23 |
| LUM4346 | FG12 | 2.37 ± 0.05 | 0.65 ± 0.03 | 341.31 ± 16.12 | 169 ± 29 | 180.0 ± 7.8 | 356 ± 23 | 356 ± 21 |
| LUM4347 | FG5 | 2.75 ± 0.03 | 0.67 ± 0.02 | 424.32 ± 7.69 | 244 ± 28 | 257.5 ± 12.3 | 421 ± 26 | 421 ± 23 |
| LUM4348 | FG16 | 2.82 ± 0.05 | 0.87 ± 0.03 | 419.26 ± 11.66 | 301 ± 38 | 301.6 ± 6.5 | 405 ± 20 | 406 ± 18 |

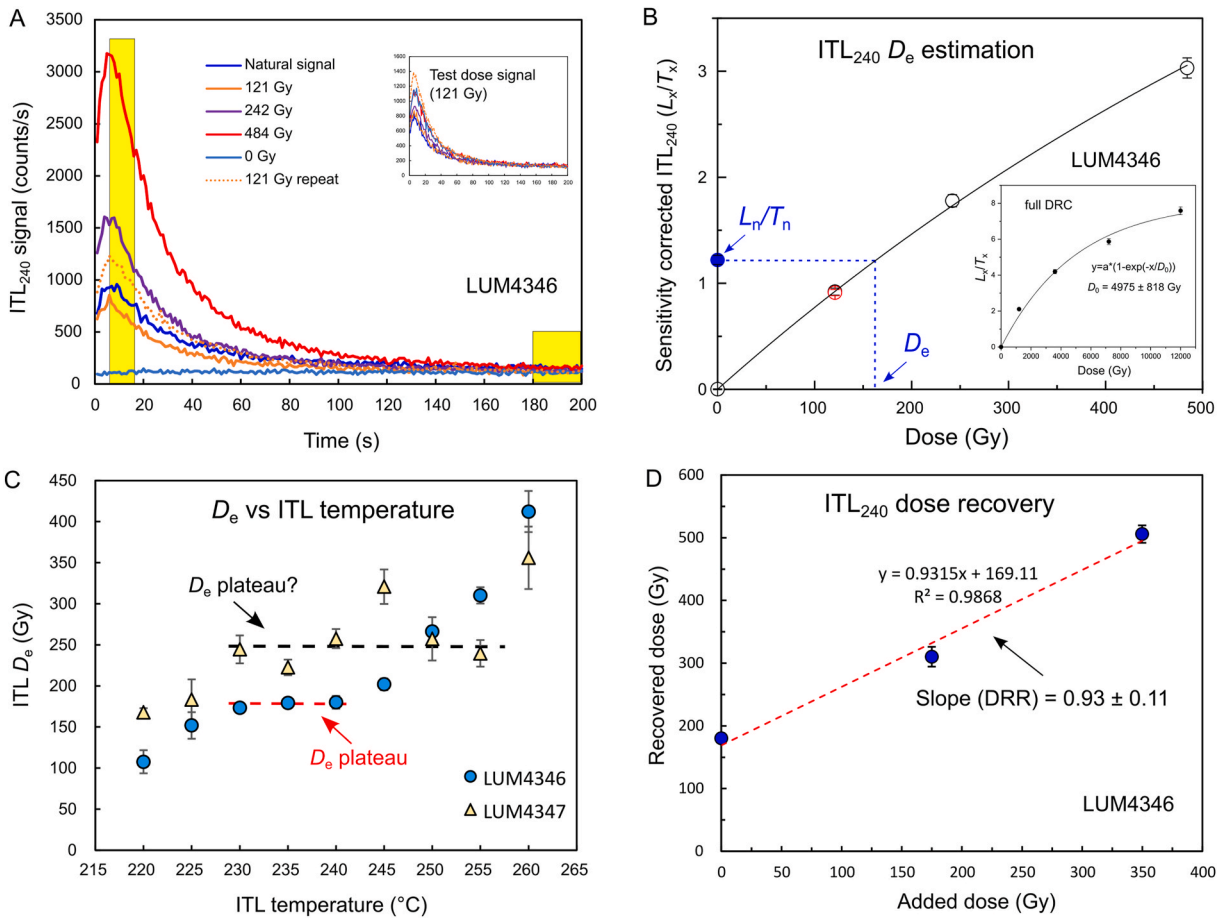


**Fig. 5.** A) $ITL_{240}$ signals for an aliquot of LUM4346. Yellow bands indicate the intervals used for signal and background. Inset graphs are the test dose signals. B) $ITL_{240}$ dose-response curve of the same aliquot in (A). The red circle is the recycling point. C) SAR $D_e$ values with ITL signals at different temperatures for LUM4346 and LUM4347. The $D_e$ at each temperature is an average of 4–8 aliquots. Error bar is 1σ. D) Dose recovery tests with the SARA protocol for $ITL_{240}$ signal of sample LUM4346. Each data point is an average of 7 aliquots. Error bar is 1σ. The slope is the dose recovery ratio (DRR).

with $\tau_{10}$ values of the 280 °C TL peak reported by previous studies (Wintle, 1974, 1977; Debenham, 1983; Engin and Güven, 1997; Stirling et al., 2012). The $\tau_{10}$ values vary by two orders of magnitude, from 2 Ma to 200 Ma, which might be sample-dependent. In our study, the $\tau_{10}$ is 109 Ma for the 280 °C TL peak. The luminescence signal can be regarded as sufficiently stable if its thermal lifetime is 10 times longer than the sample's age. As long as the sample is younger than 10 Ma, the thermal loss of the signal is negligible. In case the sample age is older than 10 Ma, a lifetime correction procedure can be applied (Adamiec et al., 2010; Duller et al., 2015; Liu et al., 2016; Tsukamoto et al., 2018; Richter et al., 2020).

### 5.3.2. *Anomalous fading*

Anomalous fading is the athermal loss of signal, which is common for the TL and IRSL signals of feldspar (Wintle, 1973; Visocekas, 1985; Spooner, 1992, 1994). The existence of anomalous fading will result in age underestimation. We performed fading tests for both the 280 °C TL peak and the $ITL_{235}$ signal.

For the 280 °C TL peak, the multiple-aliquot method was applied. A total of 25 aliquots of LUM4346 were heated to 400 °C to remove the TL signal. The aliquots were irradiated with 240 Gy, preheated to 250 °C, and divided into 4 groups. After different delay times at room temperature for the four groups, the aliquots were heated to 400 °C to record the TL signals ($L_x$). Then, the aliquots were given a test dose of 120 Gy, preheated to 250 °C and immediately heated to 400 °C to record the TL signals ($T_x$). The sensitivity corrected signals ($L_x/T_x$) of the 280 °C TL peak of the aliquots were re-normalised by the mean $L_x/T_x$ of the first group (with the shortest delay time, $t_c$), and the re-normalised signals were plotted against the delay times (Fig. S5A). The fading rate (*g*-value) was obtained from the slope of the fitted linear regression. The *g*-value ($t_c = 0.3$ h) obtained in this protocol is 0.53 ± 0.69 %.

The fading rate of the $ITL_{235}$ signal was measured following the SAR procedure (Auclair et al., 2003). After being given 240 Gy and preheated to 245 °C, the aliquot was held at room temperature for different delay times, and the $ITL_{235}$ signal was measured (Fig. S5B). A test dose of 240 Gy was given, and the $ITL_{235}$ signal of the test dose was applied for sensitivity correction. A total of five aliquots of LUM4346 were measured with this procedure. The estimated *g*-values ($t_c = 0.3$ h) varied between −2.4 %/decade to 2.2 %/decade, with a mean value of 0.03 ± 0.72 %/decade.

The fading rates of both the 280 °C TL peak and the $IL_{235}$ signal are close to 0, indicating that the TL or ITL signals have no fading. Debenham and Aitken (1984) observed no measurable signal loss of the 280 °C TL peak of stalagmitic calcite within eight months after artificial irradiation. Huang et al. (2022) reported no detectable fading of the $ITL_{235}$ signal for vein calcite crystals from a geological structure fracture. Our fading tests are consistent with previous studies, indicating that calcite samples are free of fading.

### 5.3.3. *Bleachability*

Although we applied HCl to dissolve ca. 50 % of the subsamples to remove any potential influence of light exposure, it is still in our interest to test how light exposure may affect the dating results. Thus, we performed the $ITL_{235}$ $D_e$ vs. solar bleaching test. For LUM4347, five aliquots

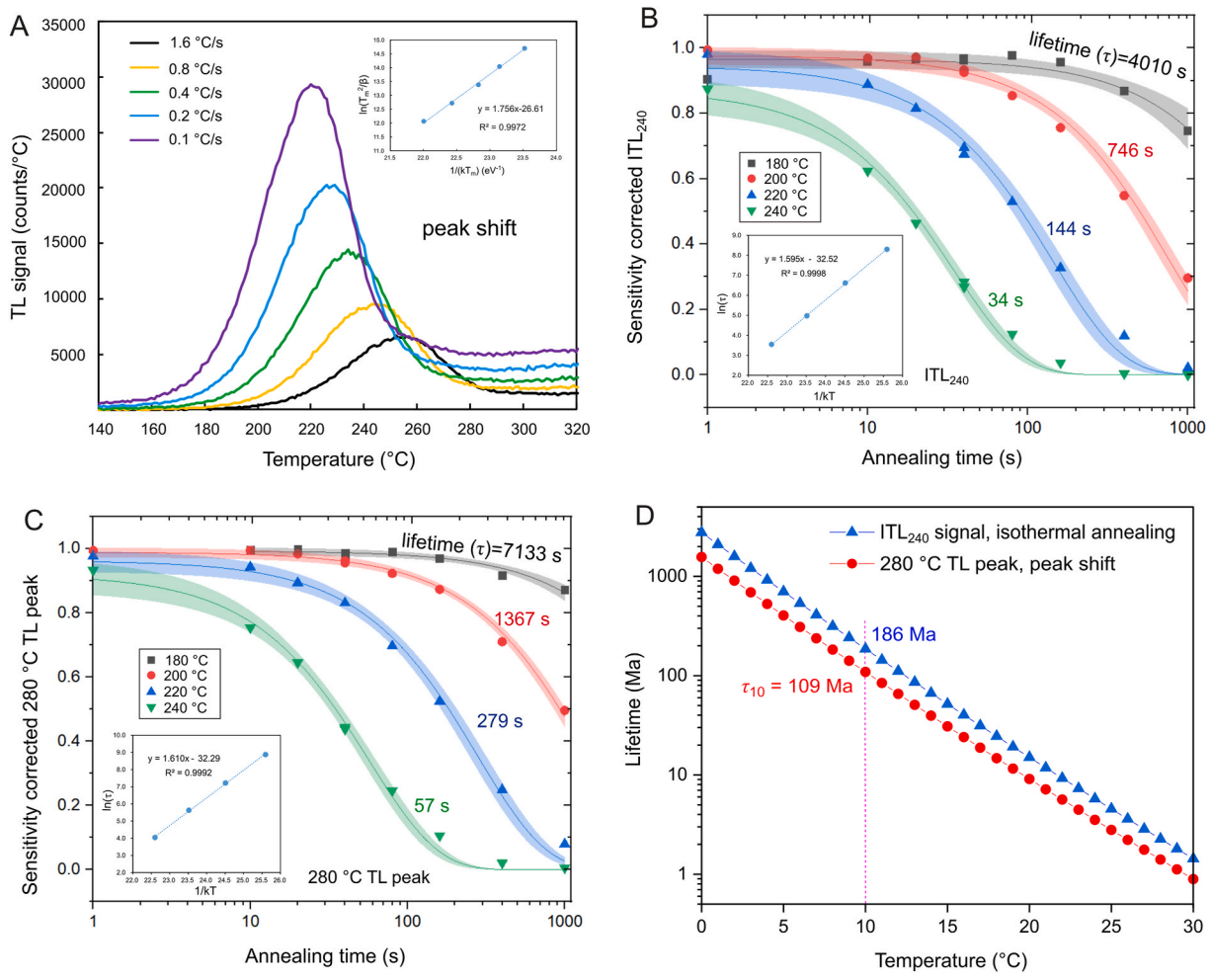


**Fig. 6.** Thermal lifetime measurements for the 280 °C TL peak and the $ITL_{240}$ signal. A) TL curves at different heating rates for one aliquot of subsample LUM4347. The inset plot is applied to obtain the trap depth ($E$) and frequency factor ($s$). B) Isothermal annealing result of the $ITL_{240}$ signal for the same aliquot. B) Isothermal annealing result of the 280 °C TL peak for the same aliquot. D) Calculated lifetimes at different temperatures, with the mean $E$ and $s$ values of all aliquots of different subsamples.

were bleached under a solar simulator (UVACUBE 400 of Dr. Hönle UV Technology) for 2 h, and the residual doses of the $ITL_{235}$ signal were measured with the SAR protocol. The mean residual $D_e$ is 119 ± 5 Gy, which is 47 % lower compared to the natural $ITL_{235}$ $D_e$ of 226 ± 10 Gy (mean of eight aliquots) (Fig. 7A). For LUM4780, three groups of aliquots (with 3 aliquots in each group) were bleached under the solar simulator for 0.5, 1 and 2 h, respectively. Contrary to LUM4347, the residual $ITL_{235}$ $D_e$ values of LUM4780 show an increasing trend with bleaching (Fig. 7A). After 2 h of bleaching, the residual $D_e$ is 147 ± 3 Gy, which is 48 % higher than the natural $ITL_{235}$ $D_e$ of 99 ± 4 Gy.

The decreasing $D_e$ with solar bleaching can be explained by the depletion of the light sensitive TL with light exposure (Liritzis, 1994; Liritzis and Bakopoulas, 1997), while the increasing $D_e$ with solar bleaching is very likely a result of phototransferred TL, which has been reported for calcite in previous studies (Ugumori and Ikeya, 1980; Lima et al., 1990; Liritzis et al., 1996; Chithambo, 2023). We suggest that, in case of solar bleaching, two processes compete with each other for the 280 °C TL peak: 1) the detrapping of charges from its own trap; 2) the re-trapping of charges evicted from a deeper trap via phototransfer (Fig. 7B). The net signal gain or loss depends on the competition between these two processes. Similar observations have also been reported by Wintle (1978). By studying the influence of light exposure (an UV lamp and a tungsten-halogen lamp) on the 275 °C TL peak of five speleothem samples, Wintle (1978) found that while three samples were not affected by light exposure, one sample showed TL increase with light exposure and one sample showed TL decrease.

To directly evaluate the phototransferred TL signal, an aliquot of LUM4347 was applied to measure the natural TL signal by heating to 400 °C (with background subtraction), and then bleached under the solar simulator by 2 h. Afterwards, the TL curve of this aliquot was measured again, and this TL curve represented the phototransferred TL (Fig. 7C). The same test was also made on an aliquot of LUM4780 (Fig. 7D). After solar bleaching, the TL peaks appeared again at ~130 °C and 300 °C. All these tests indicate that it is essential to remove the outer parts of calcite samples that have been exposed to sunlight and only use the inner parts for TL/ITL dating. Otherwise, both age underestimation and overestimation may occur.

### 5.4. Dose rate and age estimation

#### 5.4.1. U, Th, K measurements

*5.4.1.1. 'Whole rock' ICP-MS.* To measure the U, Th and K concentrations, four subsamples which are adjacent to the ITL subsamples were analysed with an ICPMS instrument in the Laboratory of the Geochemistry Research Unit at BGR. The subsamples were ground into powder in an agate mortar. After drying at 110 °C for a minimum of 12 h, powder aliquots were digested with 5M $HNO_3$ to selectively decompose the carbonate fraction (Kraemer et al., 2021). For this, 250 mg aliquots of the dried powders were weighed into acid-cleaned Savillex

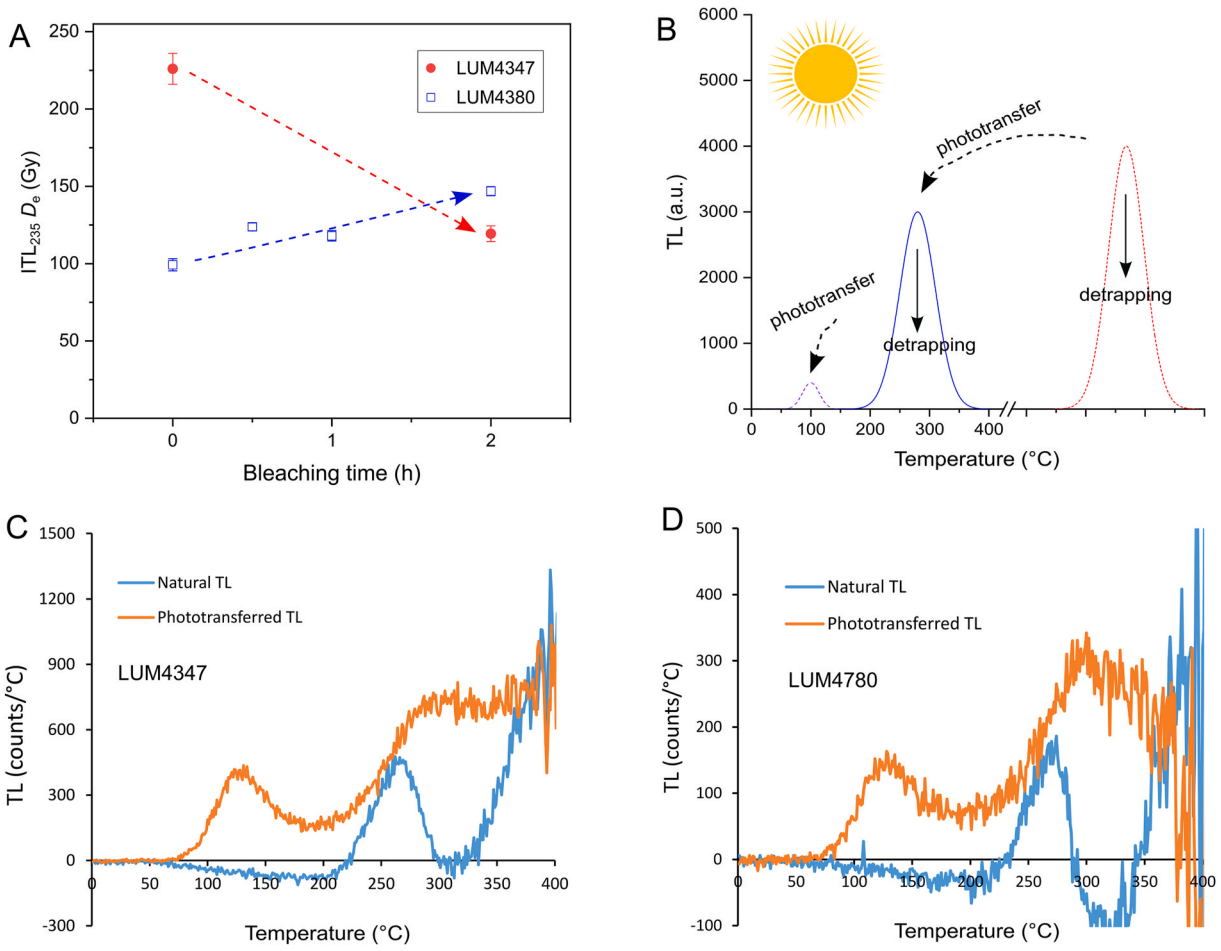


**Fig. 7.** A) $ITL_{235}$ $D_e$ variation with solar simulator bleaching. B) Schematic drawing showing the processes under solar bleaching: the signal loss of the 280 °C TL peak due to charge detrapping from its own trap and the signal increase due to phototransfer of changes from a deeper trap. C-D) Natural TL curves and phototransferred TL curves for LUM4347 and LUM4780, respectively.

PTFE beakers and 10 ml of 5M $HNO_3$ (suprapure grade) were slowly added to each beaker. The beakers were closed and the suspension was heated to 70 °C on a hotplate for 2 h. After cooling down to room temperature, the suspensions were filtered with acid/DI-cleaned filter syringes with a pore size of 0.2 μm. The filtered solutions were then diluted with DI to a final molarity of 1M $HNO_3$. For quality control, the certified reference material J-Ls1 (limestone; issued by the Geological Survey of Japan) was digested along with the samples. The carbonate extractions were measured with a Thermo Fisher iCAP TQ ICP-MS. Potassium was determined on m/z = 39 in triple quadrupole mode with oxygen as reaction gas, whilst Th and U were measured in single quadrupole mode on m/z = 232 and 238 in KED mode (kinetic energy discrimination) with He as cell gas. The elements Ru and Bi were used for internal standardisation. The measured concentrations of K in the reference standard were 63 ppm (reference: 25–83 ppm; georem Database; accessed on May 12, 2023). The measured concentrations of Th and U were 0.015 and 1.80 ppm (published literature values are 0.016 and 1.83 ppm; Dulski, 2001).

U concentrations range from 0.65 to 1.03 ppm for the four subsamples (Table 4). The concentrations of Th and K are very low, with Th concentrations between 0.007 and 0.025 ppm and K concentrations of 60–77 ppm. The dose rates from $^{232}$Th series are 0.0013–0.0045 Gy/ka and the dose rates from K are 0.0063–0.0081 Gy/ka for the four subsamples. The major contribution to the dose rate thus stems from the U series. However, the ICP-MS analyses were not directly performed on the subsamples used for ITL dating, but on the adjacent parts from the speleothem; while, the homogeneity of uranium distribution within the speleothem remains uncertain.

**Table 4**
Dose rates ($\dot{D}$) at U-series equilibrium.

| LUM ID | U[a] (ppm) | U[b] (ppm) | Th[b] (ppm) | K[b] (%) | Dose rate (Gy/ka) | | | | | |
|---|---|---|---|---|---|---|---|---|---|---|
| | | | | | Cosmic ray | Alpha | Beta | Gamma | Gamma[c] | $\dot{D} \pm 1\sigma$ |
| LUM4780 | 0.42 ± 0.02 | 0.65 ± 0.01 | 0.007 | 0.0076 | 0.051 | 0.149 | 0.068 | 0.049 | 0.010 | 0.278 ± 0.013 |
| LUM4346 | 0.65 ± 0.03 | 0.71 ± 0.02 | 0.025 | 0.0077 | 0.051 | 0.232 | 0.102 | 0.076 | 0.015 | 0.400 ± 0.019 |
| LUM4347 | 0.67 ± 0.02 | 1.03 ± 0.02 | 0.012 | 0.0067 | 0.051 | 0.238 | 0.103 | 0.077 | 0.039 | 0.431 ± 0.017 |
| LUM4348 | 0.87 ± 0.03 | 1.02 ± 0.01 | 0.008 | 0.0060 | 0.051 | 0.308 | 0.132 | 0.099 | 0.020 | 0.511 ± 0.023 |

[a] U concentrations from line scan LA-ICP-MS measurements, which are used for dose rate calculation.
[b] U, Th, K concentrations from 'whole rock' ICP-MS measurements.
[c] For LUM4780, LUM4346, LUM4348, the gamma dose rates were taken as 20 % of the gamma dose rates in infinite medium. For LUM4347, the gamma dose rate was taken as 50 % of the gamma dose rate in infinite medium.

*5.4.1.2. Line scan LA-ICP-MS.* High-resolution trace element analysis of U and Th was conducted at the Institute for Geosciences, JGU Mainz, by laser ablation inductively coupled plasma mass spectrometry (LA-ICP-MS) using an ESI New Wave NWR 193 nm ArF Excimer laser system coupled to an Agilent 7700ce ICP-MS. The analyses were conducted using the continuous line scan method with a spot size of 100 μm, a laser repetition rate of 10 Hz, a scan speed of 10 μm/s and a fluence of approximately 3.5 J/cm$^2$. For calibration, the reference material NIST SRM 610 as well as other quality control materials (NIST SRM 612, MACS-3, BCR-2G) were analysed several times during the analysis. The reproducibility based on the analyses of NIST SRM 610 was 7.2 % for Th and 12.2 % for U (1 RSD). $^{43}$Ca was used as an internal reference to calculate the trace element concentrations, and the offline data evaluation followed the calculations described in Mischel et al. (2017). For further details, the reader is referred to Jochum et al. (2012). The line scan was performed on another slice of speleothem BB2-1 which is opposite to the slice used for ITL dating. Four lines were chosen, which pass through the sampling regions of the four ITL subsamples (Fig. S6).

Line scan measurements show that the U concentrations are mostly lower than 1.0 ppm for the sample, and the Th concentrations are mostly lower than 0.2 ppm. However, there are high U, Th concentrations in the detected lines which can reach tens of or hundreds of ppm. These high U and Th concentrations tend to occur in pairs and generally correspond to high Th/U ratios (Fig. S6), which may indicate the existence of tiny detrital minerals that are abundant in U and Th. Such high U and Th spots will increase the overall U and Th concentrations. However, as the alpha particles can only penetrate 20–30 μm into the crystal, these radioactive 'hotspots' have a very small contribution to the total dose rate when the alpha irradiation dominates the dose rate. Thus, to calculate the dose rate, U concentrations exceeding 2 ppm were excluded and the remaining 'background' U concentrations were averaged (Fig. 8). After removing these spikes, the U concentrations are generally stable along the detection lines and a homogeneous medium can be assumed for dose rate calculations. The U concentrations obtained in this way are 65–92 % of the U concentrations from the 'whole-rock' ICP-MS measurements for the four subsamples.

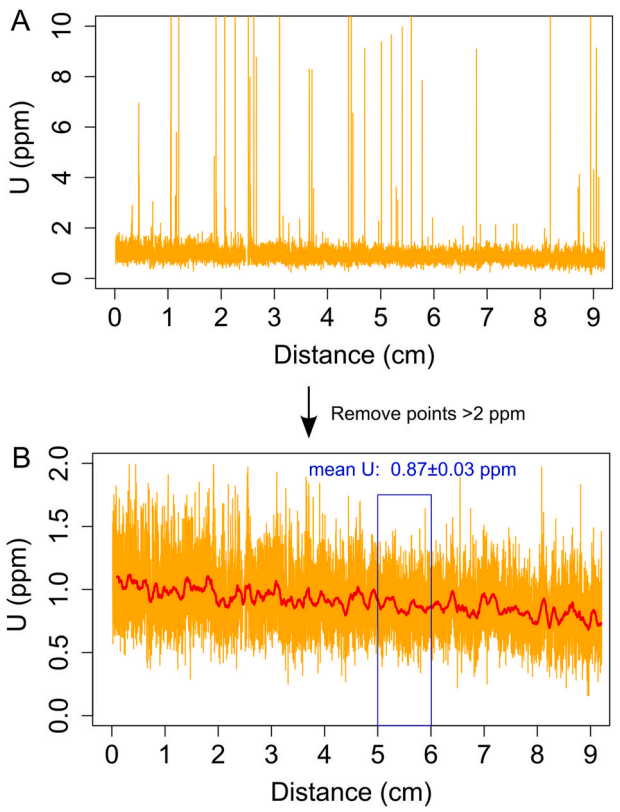


**Fig. 8.** A) U concentrations from the line scan LA-ICP-MS measurements. The line passes through the sampling position of LUM4348 (at the distance of 5–6 cm). B) U concentrations after removing the data points higher than 2 ppm. The red line indicates the average values of U concentrations over each 1 mm. The mean U for LUM4348 is calculated from the U concentrations between 5 and 6 cm distance.

*5.4.2. Alpha efficiency measurements*

As the speleothem sample is pure calcite, U is generally uniformly distributed inside and outside the grains. Consequently, the alpha dose rate has a high contribution to the total dose rate, making the alpha efficiency an important parameter. Previously reported *a*-values or *k*-values for the 280 °C TL peak of calcite vary substantially between samples (Wintle, 1978; Debenham and Aitken, 1984; Theocaris et al., 1997; Roque et al., 2001; Ogata et al., 2017; Yee and Mo, 2018; Zhang and Wang, 2020) (Fig. S7). Especially, Debenham and Aitken (1984) reported *a*-values for 27 stalagmites from two caves, which ranged from 0.09 to 0.55. Such scattered *a*-values among speleothem samples render the use of a mean *a*-value for dose rate calculation implausible. In this study, the alpha efficiency of the four subsamples used for ITL dating was measured individually.

Instead of the *a*-value system, the $S_a$ value system (Guérin and Valladas, 1980), which can directly convert the alpha flux into dose rate, was applied here. The measurements of $S_a$ values were performed in the luminescence laboratory in University Bordeaux Montaigne, with an inhouse-built alpha irradiator ($^{241}$Am foil source). The alpha flux rate of the source has been accurately calibrated to be 1.9*10$^5$ α-particles s$^{-1}$ cm$^{-2}$ (Kreutzer et al., 2018). The speleothem samples were ground into fine grained powders and the 4–11 μm fraction was separated following Stokes law. Aliquots were prepared with steel cups from Freiberg Instruments, with ca. 0.6 mg sample on each cup. In this way, the covered cup surface is thin-layered, with an average surface density of 1 mg cm$^{-2}$ (Kreutzer et al., 2018).

The luminescence measurements were performed on a Lexsyg smart TL/OSL reader (always with $N_2$ flow). The built-in beta source of the reader is 0.133 Gy/s for fine grains (4–11 μm) on the steel cups. The signals were detected by a HAMAMATSU H7360-02 photomultiplier tube through a 2 mm thick Schott BG-39 filter. The aliquots were heated to 450 °C (5 °C/s) for four times (without background subtraction) to remove the natural signal and the spurious signal completely. Afterwards, the aliquots were given a dose of ca. 88 Gy and heated to 450 °C. Repeat the dosing and heating step for two more times. In this way, the aliquots were 'stabilised' and sensitivity change in the following measurements will be smaller. The stabilised aliquots were put under the alpha source for irradiation of 12 h. The alpha flux received by the aliquots was 8.21*10$^9$ α-particles cm$^{-2}$. After alpha irradiation, the corresponded beta $D_e$ was measured following a TL SAR protocol (Table S2). As these aliquots were already stabilised by repeated dosing and heating, the SAR protocol can still be applied for TL $D_e$ measurements. To reduce the influence of regenerated spurious signal, which can regenerate during the storage (Pagonis et al., 1997), the time lag between the alpha irradiation and $D_e$ measurements was less than one day. The heating rate was set as 1 °C/s, to make the 280 °C TL peak (with heating rate of 5 °C/s) shifted to approximately 245 °C, to further reduce the influence of spurious TL signal (Fig. S8). The beta $D_e$ was divided by the given alpha flux to get the $S_a$ value (Table S3). For the four subsamples, the $S_a$ values are quite close to each other, ranging from 19.4 to 21.9 μGy/(1000α*cm$^{-2}$). The mean $S_a$ value of the four subsamples is 20.8 ± 0.5 μGy/(1000α*cm$^{-2}$). We suspect that the variation of the $S_a$ values between the four subsamples results from the random error of measurements, as only 2 to 3 aliquots were measured for each subsample. Thus, the mean $S_a$ value was applied for dose rate calculation. If converting the $S_a$ value into *k*-value system, the mean effective *k*-value for U ($k_{eff}$_U) would be 0.126 ± 0.003, and for Th ($k_{eff}$_Th) 0.140 ± 0.003 (details of conversion in Table S3 notes).

*5.4.3. Dose rates at equilibrium*

Our measured $S_a$ values were used for alpha dose rate calculation, and conversion factors from Guérin et al. (2011) were used for beta and gamma dose rate calculation. Alpha and beta dose rates were calculated based on an infinite homogeneous medium. Attenuation of the gamma dose rate was considered because the speleothem sample is not big enough in size, taking into account that the gamma ray has a travelling length of around 30 cm in rocks. Due to the irregular shape of the speleothem sample, accurate gamma attenuation factors for the four subsamples are difficult to estimate. We applied a gamma attenuation factor of 0.2 for the three subsamples at the rim (LUM4346, LUM4348, LUM4780) and of 0.5 for the subsample in the centre (LUM4347). To account for the large uncertainty, a relative error of 50 % was assumed for the gamma dose rate. It is noteworthy that the gamma dose rate assuming an infinite medium contributes only ~13 % to the total dose rate, and thus the ages are not sensitive to the gamma attenuation factors. Cosmic ray dose rate was calculated to be 0.051 Gy/ka based on an overburden thickness of 10 m and a rock density of 2.7 g/cm$^3$ (Prescott and Hutton, 1994). Although Th and K have very small contribution to the total dose rate (0.008–0.013 Gy/ka) due to their low concentrations, they were still considered in the dose rate calculation. The U concentrations measured along lines with the LA-ICP-MS method were used for dose rate calculation. The total dose rates at U-series equilibrium are presented in Table 4. For all the four subsamples, the alpha irradiation contributes to 62–65 % of the total dose rate (Fig. S9).

*5.4.4. Dose rate simulation and ages*

The total dose rate is mainly determined by the $^{238}$U series. However, the $^{238}$U decay chain is not always in secular equilibrium since $^{230}$Th was absent at the time of speleothem crystallisation, and the initial activity ratio of $^{234}$U and $^{238}$U ($[^{234}U/^{238}U]_0$) in dripwater can be much higher than 1 (Cowart and Osmond, 1977; Osmond et al., 1983; Plater et al., 1992; Tripathi et al., 2013). As a result, the dose rate changes with time. Here we applied two methods to tackle the problem of dose rate variation.

One method is to directly model the dose rate and $D_e$ variation with time. Fig. 9 shows examples for LUM4347 and LUM4780. We simulated the radioactivity of the $^{238}$U, $^{234}$U and $^{230}$Th isotopes with a step of one year using numerical simulation, following the initial activities and decay constants. The [$^{238}$U] activity is almost a constant. Since the $[^{234}U/^{238}U]_0$ is larger than 1, the [$^{234}$U] decreases with time, and consequently the [$^{230}$Th] initially increases and then decreases with time (Fig. 9A). The dose rate of the $^{238}$U decay chain was calculated by dividing the chain into three segments ($^{238}$U–$^{234}$U, $^{234}$U to $^{230}$Th, $^{230}$Th to the $^{206}$Pb), and corresponding conversion factors (Guérin et al., 2011) in each segment were used. As the two daughter isotopes between $^{238}$U and $^{234}$U, and all daughter isotopes behind $^{230}$Th have short half-lives compared to the sample age, instant equilibrium can be assumed for each segment. The dose rate of each segment is calculated and summed up to get the dose rate of the whole $^{238}$U series (Fig. 9B). The dose rate from $^{232}$Th series, $^{40}$K and the cosmic dose rate were also calculated and added to get the total dose rate (annual dose). For sample LUM4347, the annual rate was 0.189 Gy/ka at the crystallisation of speleothem. Then it increased with time and reached a peak value of 0.694 Gy/ka at 229 ka. Afterwards, it decreased again and will eventually reach a steady state of 0.425 Gy/ka. By adding up those annual doses, the growth pattern of $D_e$

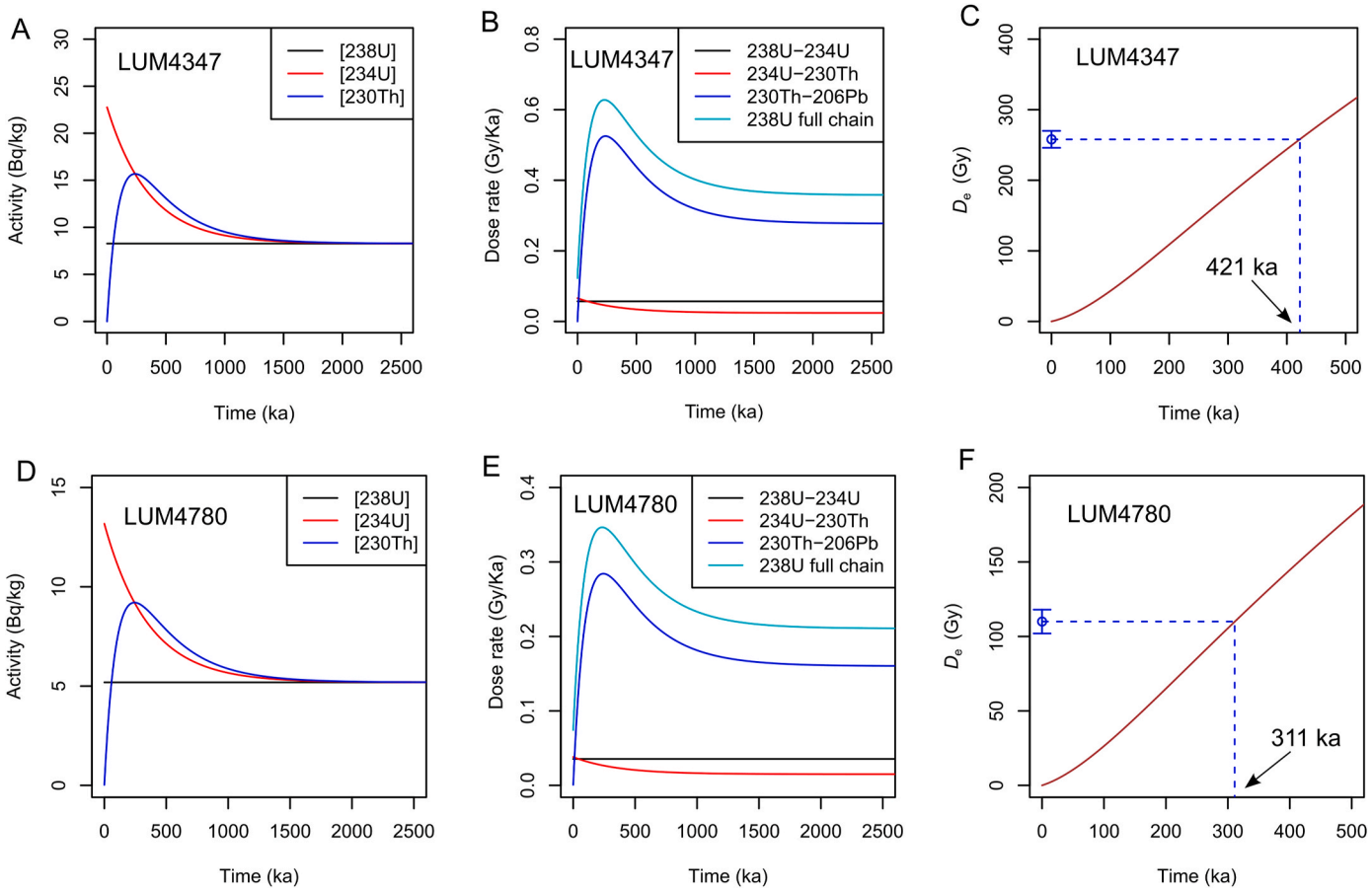


**Fig. 9.** Dose rate simulation for LUM4347 and LUM4780. A) Radioisotope activities of $^{238}$U, $^{234}$U and $^{230}$Th with time for LUM4347. The $[^{234}U/^{238}U]_0$ is 2.75; B) Time-dependent variation of dose rates within the three segments ($^{238}$U–$^{234}$U, $^{234}$U to $^{230}$Th, $^{230}$Th to $^{206}$Pb) of the $^{238}$U decay chain for LUM4347; C) Growth of equivalent dose ($D_e$) with time for LUM4347. D-F are the same as A-C, but for LUM4780. Note that the U-series reach equilibrium only after ca. 1.5 Ma, and the dose rates become stable afterwards.

with age can be obtained (Fig. 9C). The measured $D_e$ of LUM4347 is 257.5 Gy, which corresponds to an age of 421 ka. For the error of the ages, the Monte Carlo method was applied, taking into consideration of four normal distributions: the U concentration, the $[^{234}U/^{238}U]_0$, the $S_a$ value and the $D_e$ value. 300 simulations were applied to get a normal distribution of the ages, and the standard deviation (1σ) was deduced (Fig. S10). The ITL age deduced in this way is termed *simulated age*. Note that the $^{226}Ra$ behind $^{230}Th$ has a half-life of 1602 years, which is not sufficiently short for very young samples (e.g., <10 ka). Dose rate simulation with 4-segment division was tested and the *simulated age* increased by less than 2 ka, which is negligible considering the sample ages in this study. As a result, 3-segment simulation is used throughout this study.

The other method is the age iteration method modified from Ikeya and Ohmura (1983). Firstly, the total dose rate at U-series equilibrium ($\dot{D}$) was calculated. An initial age was calculated dividing the measured $D_e$ with $\dot{D}$. The following iterative calculation was performed.

1) Calculated the $D_e$_cal with equation:

$$D_e\_cal = \dot{D}\cdot age + \dot{D}_{234}\cdot(r_0-1)\cdot\left(1-e^{-\lambda^{234}age}\right)\Big/\lambda^{234} - \dot{D}_{230}\cdot\left\{\left(1-e^{-\lambda^{230}age}\right)\Big/\lambda^{230} - 1\Big/\lambda^{234}\cdot(r_0-1)\cdot\left[1-\left(\lambda^{230}\cdot e^{-\lambda^{234}age}-\lambda^{234}\cdot e^{-\lambda^{230}age}\right)\Big/\left(\lambda^{230}-\lambda^{234}\right)\right]\right\} \quad (1)$$

where $\dot{D}_{234}$ is the dose rate in the decay chain between the $^{234}U$ and $^{230}Th$, and $\dot{D}_{230}$ is the dose rate in the decay chain after $^{230}Th$. The $\lambda^{234}$ and $\lambda^{230}$ are the decay constants of the $^{234}U$ and $^{230}Th$, respectively and $r_0$ is the $[^{234}U/^{238}U]_0$.

2) Calculated a new age:

$$age = age^{*}D_e/D_e\_cal \quad (2)$$

where $D_e$ is the measured value, which is a constant.

3) Back to step 1.

The age became stable after approximately five times of iteration. The age obtained in this way is termed *iterated age*, and we assume the same relative errors for the *iterated age* as the initial age.

The *iterated ages* and *simulated ages* of all subsamples based on the $ITL_{240}$ signal are shown in Table 3.

## 6. Discussion

The $D_e$ values obtained by the MAAD protocol with the 280 °C TL peak and the SAR protocol with the $ITL_{240}$ signal agree well with each other. However, the $ITL_{240}$ SAR $D_e$ values have much smaller errors compared to the TL MAAD $D_e$ values, as the SAR protocol avoids the error stemming from inter-aliquot variation. For the samples in this study, the spurious TL signal in the high temperature range is not significant, so the accurate MAAD $D_e$ estimation with the 280 °C TL peak is still achievable.

The $ITL_{240}$ ages obtained by both the dose rate simulation method and age iteration method are identical, which further proves the reliability of the two correction methods. Mathematically, the age iteration method and the dose rate simulation method are similar. The iteration method uses integration, which theoretically divides the time into infinitely small intervals. In the dose rate simulation method, we divide the time into 1-year intervals. The consistent age estimates indicate that the 1-year interval in dose rate simulation has a sufficiently high resolution. The age iteration method is more convenient compared to the dose rate simulation method. However, the age iteration method can only be applied to closed systems, as in the case of speleothems, while the dose rate simulation method can be applied to open systems because it is more flexible and offers potential to incorporate U-uptake, Rn loss, etc. The ITL ages are plotted against the Th/U ages in Fig. 10. For all subsamples, the ITL ages are consistent with the $^{230}Th/U$ ages considering the errors, indicating the reliability of the ITL dating method on speleothems.

As shown in the above section, accurate ITL age estimation requires the $[^{234}U/^{238}U]_0$ value. Because of the long residence time of U in seawater, the $[^{234}U]/[^{238}U]$ in seawater remains to be around 1.14 (Chen et al., 1986). However, terrestrial waters have variable $[^{234}U]/[^{238}U]$ values depending on weathering and infiltration conditions, which can range from 0 to more than 10, with the majority of the values between 1 and 3 (Cowart and Osmond, 1977; Osmond et al., 1983). If ignoring the U-series disequilibrium and simply applying the dose rate at secular equilibrium for age estimation, the age can thus be substantially over- or underestimated (Fig. 11). To obtain the $[^{234}U/^{238}U]_0$ value, accurate measurements of the present concentrations of $^{234}U$, $^{238}U$ and $^{230}Th$ are needed. However, these measurements are already the basis of the much more accurate $^{230}Th/U$ dating method. The much higher errors of the ITL ages makes ITL dating not competitive when compared to $^{230}Th/U$ dating for speleothem samples younger than 600 ka and without substantial detrital Th contamination. However, contrary to $^{230}Th/U$ dating, detrital Th contamination is not a drawback but rather an advantage for ITL dating because it reduces the relative error of the total dose rate brought in by U-series disequilibrium. This means that ITL dating offers an alternative dating method for speleothems that are contaminated with substantial amounts of detrital Th and

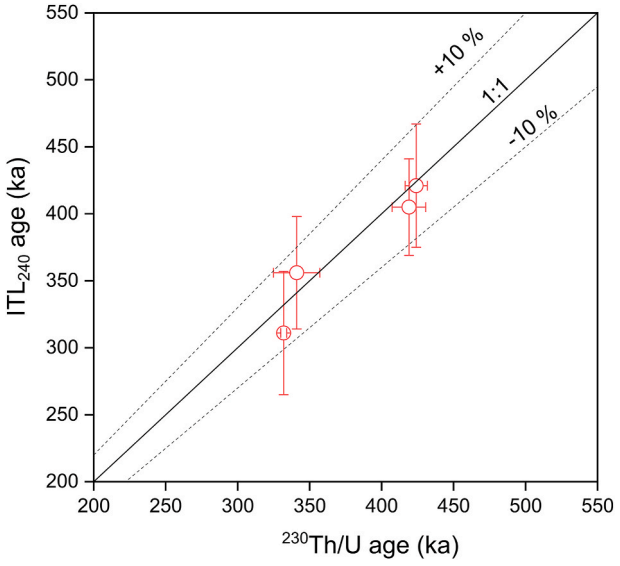


**Fig. 10.** Comparison of the ITL ages with the $^{230}Th/U$ ages. Error bars are 2σ for all ages.

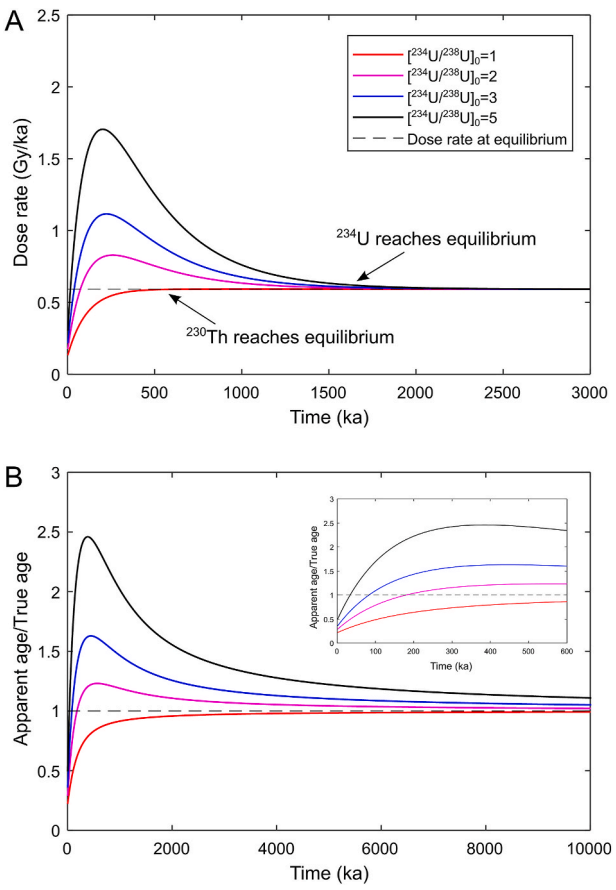


**Fig. 11.** A) Dose rate (1 ppm $^{238}$U) variation over time since the crystallisation of a speleothem with different initial [$^{234}$U/$^{238}$U] activity ratios; B) Ratio of the apparent age (assuming a constant dose rate as it is always in secular equilibrium) and the true age with the time since crystallisation. The inset plot shows the first 600 ka.

cannot be reliably dated with U-series methods. Yet, the major advantage of ITL dating is its higher dating limit. The $D_0$ of the $ITL_{240}$ signal of the speleothem sample is 4975 ± 818 Gy. Such high $D_0$ values have been reported for the 280 °C TL peak of snail opercula (Duller et al., 2009; Stirling et al., 2012) and ITL signals for travertine, limestone and calcite veins (Zhang and Wang, 2020; Huang et al., 2022), indicating the overall high saturation dose for calcite with different rock types. Assuming a dating limit of $2D_0$ (Wintle and Murray, 2006), the maximum $D_e$ of calcite, which can be measured with high reliability, would be ~10000 Gy. Assuming a dose rate of 0.5 Gy/ka (from Table 4), the maximum dating range can reach 20 Ma, thus offering a pathway to date samples too old for $^{230}$Th/U dating and/or unsuitable for U-Pb methods. The ideal application case would be speleothem samples which have both a younger part suitable for $^{230}$Th/U dating and an older part formed beyond the limit of the $^{230}$Th/U method but amenable to ITL dating (Fig. 12). From $^{230}$Th/U dating on the younger part, a [$^{234}$U/$^{238}$U]$_0$ value can be obtained. If the [$^{234}$U/$^{238}$U]$_0$ does not change much with time for the same speleothem sample, [$^{234}$U/$^{238}$U]$_0$ of the younger part of the speleothem can be used when applying ITL dating on the older part.

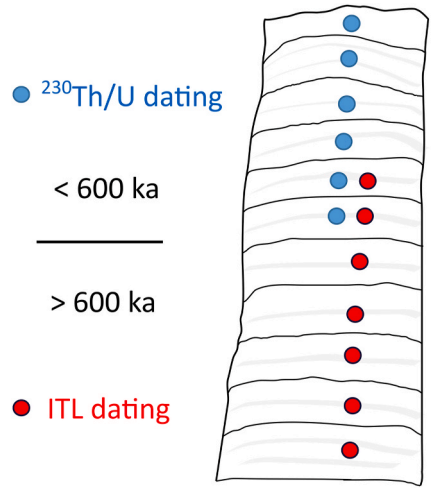


**Fig. 12.** An ideal speleothem sample which can be dated by a combination of $^{230}$Th/U and ITL methods. The [$^{234}$U/$^{238}$U]$_0$ value deduced from $^{230}$Th/U dating in the younger part (<600 ka) of the speleothem sample can be used for the older part with ITL dating.

For speleothem samples which have no younger part suitable for $^{230}$Th/U dating, a feasible way is to assume the [$^{234}$U/$^{238}$U]$_0$ value and combine $^{234}$U/$^{238}$U dating and ITL dating. With the assumed [$^{234}$U/$^{238}$U]$_0$ value and modern [$^{234}$U/$^{238}$U], an $^{234}$U/$^{238}$U age can be calculated. Meanwhile, an ITL age can also be obtained with the [$^{234}$U/$^{238}$U]$_0$. With a higher [$^{234}$U/$^{238}$U]$_0$, the $^{234}$U/$^{238}$U age would be higher, while the ITL age would be lower due to the overall higher dose rate (the measured $D_e$ is a constant). If the $^{234}$U/$^{238}$U age is older than ITL age, it means that the assumed [$^{234}$U/$^{238}$U]$_0$ is too high, and vice visa. We can moderate the [$^{234}$U/$^{238}$U]$_0$ value until the $^{234}$U/$^{238}$U age and the ITL age agree with each other. This method is only valid for samples within the dating range of the $^{234}$U/$^{238}$U dating method (i.e., <1.5 Ma). However, for very old speleothem samples (e.g., >5 Ma), the age determination will not rely heavily on the [$^{234}$U/$^{238}$U]$_0$ value, and it is plausible to assume secular equilibrium since the crystallisation. Assuming a [$^{234}$U/$^{238}$U]$_0$ value of 2, an age calculated assuming secular equilibrium since crystallisation would only be 4 % older than the true age for a true age of 5 Ma. This overestimation reduces to 2 % if the true age is 10 Ma (Fig. 11B). For a [$^{234}$U/$^{238}$U]$_0$ value of 3 (higher than the values of drip water observed in most caves), the overestimation would be 10 % for a true age of 5 Ma and 5 % for a true age of 10 Ma.

The TL signal of our speleothem sample has a lifetime of ~100 Ma at a cave temperature of 10 °C. For samples older than 10 Ma, a thermal loss correction needs to be applied on the ages, which will bring in additional uncertainty. However, the lifetime increases substantially with lower temperature. At a cave temperature of 5 °C, the lifetime increases to ~400 Ma, which can theoretically increase the dating limit to 40 Ma if the dose rate is low (<0.25 Gy/ka). Thus, it would also be advantageous to date speleothems from colder regions. For old samples beyond the limit of $^{230}$Th/U dating, U-Pb dating is only applicable for samples with high U and low common Pb. Contrarily, the low U concentration will be an advantage for ITL dating on old speleothems, as the low dose rate will make the maximum age limit higher.

The subsamples used in this study are ca. 5 g, which are quite large compared to typical samples used for $^{230}$Th/U-dating. The large sample size prohibits high spatial resolution dating of speleothems with the ITL signal. The speleothem used in this study grew fast at two stages, and the ages within each stage are very close to each other. Thus, it is still reasonable to take large subsamples for ITL dating. However, when a speleothem grew very slowly, a large subsample will span a long growth period. It would also be problematic to use a mean U concentration for dose rate calculation if U concentration varies significantly between different growth bands. To achieve a high spatial resolution by ITL dating, a feasible approach would be to use the method employed in rock surface dating, which involves drilling a 10 mm-diameter core and cutting the core into 0.5–1.0 mm thick slices under subdued red light (e.g., Sohbati et al., 2011; Luo et al., 2018; Elkadi et al., 2021). Each thin slice would then provide one ITL age.

## 7. Conclusions

The $ITL_{240}$ signal can isolate the 280 °C TL peak with little contribution of TL signals from the higher temperature range, which is advantageous for dating calcite samples with highly spurious signals. The speleothem sample tested here has only a limited spurious signal, thus the SAR $D_e$ values of the $ITL_{240}$ signal are consistent with the MAAD $D_e$ of the 280 °C TL peak. However, the use of the single-aliquot technique results in much smaller error estimates for the $ITL_{240}$ SAR $D_e$ values.

Alpha efficiencies of the four subsamples are quite close to each other, with a mean $S_a$ value of 20.8 ± 0.5 μGy/(1000α*$cm^{-2}$). Line scan LA-ICP-MS measurements show spikes in U distribution. Removing these high U concentrations, the dose rate can be calculated using an infinite homogeneous medium. The dose rate variation due to U-series disequilibrium can be simulated with the initial $^{238}U$, $^{234}U$, $^{230}Th$ activities and their decay constants. For the four tested subsamples, the $ITL_{240}$ ages are always consistent with $^{230}Th/U$ ages, confirming the reliability of the ITL dating method. Due to the higher uncertainties, ITL dating is not comparable to $^{230}Th/U$ dating for samples younger than 600 ka. However, ITL dating provides a new avenue for dating speleothem samples older than the $^{230}Th/U$ dating limit and samples with detrital Th contamination (in case of U-Th dating) and common lead contamination (in case of U-Pb dating). This method offers an alternative promising approach for deep-time speleothem-based geochronology.

## CRediT authorship contribution statement

**Junjie Zhang:** Writing – original draft, Visualization, Validation, Project administration, Methodology, Investigation, Funding acquisition, Formal analysis, Data curation, Conceptualization. **Jennifer Klose:** Writing – review & editing, Visualization, Validation, Methodology, Investigation, Formal analysis, Data curation. **Denis Scholz:** Writing – review & editing, Funding acquisition, Conceptualization. **Norbert Marwan:** Writing – review & editing, Funding acquisition, Conceptualization. **Sebastian F.M. Breitenbach:** Writing – review & editing, Conceptualization. **Lutz Katzschmann:** Writing – review & editing, Validation, Resources. **Dennis Kraemer:** Writing – review & editing, Validation, Data curation. **Sumiko Tsukamoto:** Writing – review & editing, Supervision, Conceptualization.

## Declaration of competing interest

The authors declare that they have no known competing financial interests or personal relationships that could have appeared to influence the work reported in this paper.

## Data availability

Data will be made available on request.

## Acknowledgements

J. Zhang and S. Tsukamoto are grateful to Nobert Mercier, Sebastian Kreutzer and Chantal Tribolo for their help and discussion about alpha efficiency measurements and evaluation. The help from Antje Wittenberg, Melanie Sierralta and Dieter Rammlmair for μ-EDXRF measurements, and the help from Niko Götze and Kristian Ufer for XRD analyses are sincerely appreciated. D. Scholz and J. Klose are thankful to M. Großkopf, M. Weber, and V. Blumrich for assistance during U-series dating at the University of Mainz. This study is funded by the German Research Foundation (Deutsche Forschungsgemeinschaft, DFG) as project number 508966574 (MA 4759/18-1, SCHO 1274/17-1, ZH 1184/2-1). D. Scholz is also thankful to the DFG for funding through grant INST 247/889 FUGG.

## Appendix A. Supplementary data

Supplementary data to this article can be found online at https://doi.org/10.1016/j.quageo.2024.101628.

## References

Adamiec, G., Duller, G.A.T., Roberts, H.M., Wintle, A.G., 2010. Improving the TT-OSL SAR protocol through source trap characterisation. Radiat. Meas. 45, 768–777.
Aitken, M.J., 1985. Thermoluminescence Dating. Academic Press, London.
Aitken, M.J., Bussell, G.D., 1979. Zero-glow monitoring (ZGM). Ancient TL 6, 13–15.
Aitken, M.J., Bussell, G.D., 1982. TL dating of fallen stalactites. PACT 6, 550–554.
Aitken, M.J., Wintle, A.G., 1977. Thermoluminescence dating of calcite and burnt flint - age relation for slices. Archaeometry 19, 100–105.
Auclair, M., Lamothe, M., Huot, S., 2003. Measurement of anomalous fading for feldspar IRSL using SAR. Radiat. Meas. 37, 487–492.
Bangert, U., Hennig, G.J., 1979. Effect of sample preparation and the influence of clay impurities on the TL-dating of calcitic cave deposits. PACT 3, 281–289.
Breitenbach, S.F.M., Plessen, B., Waltgenbach, S., Tjallingii, R., Leonhardt, J., Jochum, K. P., Meyer, H., Goswami, B., Marwan, N., Scholz, D., 2019. Holocene interaction of maritime and continental climate in Central Europe: new speleothem evidence from Central Germany. Glob. Planet. Change 176, 144–161.
Buylaert, J.P., Murray, A.S., Huot, S., Vriend, M.G.A., Vandenberghe, D., De Corte, F., Van den haute, P., 2006. A comparison of quartz OSL and isothermal TL measurements on Chinese loess. Radiat. Prot. Dosi. 119, 474–478.
Chen, J.H., Lawrence Edwards, R., Wasserburg, G.J., 1986. 238U,234U and232Th in seawater. Earth Planet Sci. Lett. 80, 241–251.
Cheng, H., Edwards, R.L., Shen, C.-C., Polyak, V.J., Asmerom, Y., Woodhead, J., Hellstrom, J., Wang, Y., Kong, X., Spötl, C., 2013. Improvements in 230Th dating, 230Th and 234U half-life values, and U–Th isotopic measurements by multi-collector inductively coupled plasma mass spectrometry. Earth Planet Sci. Lett. 371, 82–91.
Cheng, H., Edwards, R.L., Sinha, A., Spotl, C., Yi, L., Chen, S.T., Kelly, M., Kathayat, G., Wang, X.F., Li, X.L., Kong, X.G., Wang, Y.J., Ning, Y.F., Zhang, H.W., 2016. The Asian monsoon over the past 640,000 years and ice age terminations. Nature 534, 640–646.
Chithambo, M.L., 2023. Phototransferred thermoluminescence of calcite: analysis and mechanisms. J. Appl. Phys. 134, 055109.
Choi, J.H., Murray, A.S., Cheong, C.S., Hong, D.G., Chang, H.W., 2006. Estimation of equivalent dose using quartz isothermal TL and the SAR procedure. Quat. Geochronol. 1, 101–108.
Cowart, J.B., Osmond, J.K., 1977. Uranium isotopes in groundwater: their use in prospecting for sandstone-type uranium deposits. In: Butt, C.R.M., Wilding, I.G.P. (Eds.), Developments in Economic Geology. Elsevier, pp. 365–379.
Debenham, N.C., 1983. Reliability of thermoluminescence dating of stalagmitic calcite. Nature 304, 154–156.
Debenham, N.C., Aitken, M.J., 1984. Thermoluminescence dating of stalagmitic calcite. Archaeometry 26, 155–170.
Domínguez-Villar, D., Fairchild, I.J., Baker, A., Carrasco, R.M., Pedraza, J., 2013. Reconstruction of cave air temperature based on surface atmosphere temperature and vegetation changes: implications for speleothem palaeoclimate records. Earth Planet Sci. Lett. 369–370, 158–168.
Duller, G.A.T., Penkman, K.E.H., Wintle, A.G., 2009. Assessing the potential for using biogenic calcites as dosemeters for luminescence dating. Radiat. Meas. 44, 429–433.
Duller, G.A.T., Tooth, S., Barham, L., Tsukamoto, S., 2015. New investigations at Kalambo Falls, Zambia: luminescence chronology, site formation, and archaeological significance. J. Hum. Evol. 85, 111–125.
Dulski, P., 2001. Reference materials for geochemical studies: new analytical data by ICP-ms and critical discussion of reference values. Geostand. Geoanal. Res. 25, 87–125.
Elkadi, J., King, G.E., Lehmann, B., Herman, F., 2021. Reducing variability in OSL rock surface dating profiles. Quat. Geochronol. 64, 101169.
Engin, B., Güven, O., 1997. Thermoluminescence dating of Denizli travertines from the southwestern part of Turkey. Appl. Radiat. Isot. 48, 1257–1264.
Franklin, A.D., Hornyak, W.F., Tschirgi, A.A., 1988. Thermo-luminescence dating of tertiary period calcite. Quat. Sci. Rev. 7, 361–365.
Guérin, G., Mercier, N., Adamiec, G., 2011. Dose-rate conversion factors: update. Ancient TL 29, 5–8.
Henderson, G.M., 2006. Caving in to new chronologies. Science 313, 620–622.
Hoogenstraaten, W., 1958. Electron traps in zinc-sulphide phosphors. Philips Res. Rep. 13, 515–693.
Huang, C., Zhang, J., Wang, L., Zhao, H., Li, S.-H., 2022. Equivalent dose estimation of calcite using isothermal thermoluminescence signals. Quat. Geochronol. 70, 101310.
Ikeya, M., Ohmura, K., 1983. Comparison of ESR ages of corals from marine terraces with $^{14}C$ and $^{230}Th/^{234}U$ ages. Earth Planet Sci. Lett. 65, 34–38.
Jochum, K.P., Scholz, D., Stoll, B., Weis, U., Wilson, S.A., Yang, Q., Schwalb, A., Börner, N., Jacob, D.E., Andreae, M.O., 2012. Accurate trace element analysis of speleothems and biogenic calcium carbonates by LA-ICP-MS. Chem. Geol. 318–319, 31–44.
Kraemer, D., Frei, R., Ernst, D.M., Bau, M., Melchiorre, E., 2021. Serpentinization in the Archean and Early Phanerozoic – insights from chromium isotope and REY systematics of the Mg Cr hydroxycarbonate stichtite and associated host serpentinites. Chem. Geol. 565, 120055.
Kreutzer, S., Martin, L., Dubernet, S., Mercier, N., 2018. The IR-RF alpha-Efficiency of K-feldspar. Radiat. Meas. 120, 148–156.

Liao, J., Hu, C., Li, C., Zhang, G., Gao, J., Huang, J., 2014. Spurious thermoluminescence from stalagmite: a new paleoenvironmental proxy. Earth Sci. 23 (4), 443–450.
Lima, J.F., Trzesniak, P., Yoshimura, E.M., Okuno, E., 1990. Phototransferred thermoluminescence in calcite. Radiat. Prot. Dosimetry 33, 143–146.
Liritzis, I., 1994. A new dating method by thermoluminescence of carved megalithic stone building. Comptes Rendus de l'Académie des Sciences Paris, serie II 319, 603–610.
Liritzis, I., Guibert, P., Foti, F., Schvoerer, M., 1996. Solar bleaching of thermoluminescence of calcites. Nucl. Instrum. Methods Phys. Res. B 117, 260–268.
Liritzis, I., Bakopoulos, Y., 1997. Functional behaviour of solar bleached thermoluminescence in calcites. Nucl. Instrum. Methods Phys. Res. B 132, 87–92.
Liu, J.F., Murray, A.S., Buylaert, J.P., Jain, M., Chen, J., Lu, Y., 2016. Stability of fine-grained TT-OSL and post-IR IRSL signals from a *c.* 1 Ma sequence of aeolian and lacustrine deposits from the Nihewan Basin (northern China). Boreas 45, 703–714.
Luo, M., Chen, J., Liu, J., Qin, J., Owen, L.A., Han, F., Yang, H., Wang, H., Zhang, B., Yin, J., Li, Y., 2018. A test of rock surface luminescence dating using glaciofluvial boulders from the Chinese Pamir. Radiat. Meas. 120, 290–297.
McDougall, D.J., 1968. Thermoluminescence of Geological Materials. Academic Press, New York.
Mejdahl, V., Bøtter-Jensen, L., 1994. Luminescence dating of archaeological materials using a new technique based on single aliquot measurements. Quat. Sci. Rev. 13, 551–554.
Mischel, S.A., Mertz-Kraus, R., Jochum, K.P., Scholz, D., 2017. Termite - an R script for fast reduction of LA-ICPMS data and its application to trace element measurements. Rapid Commun. Mass Spectrom. 31, 1079–1087.
Moore, G.W., 1952. Speleothem—a New Cave Term, vol. 10. National Speleological Society News, p. 2.
Murray, A.S., Wintle, A.G., 2000. Application of the single-aliquot regenerative-dose protocol to the 375 °C quartz TL signal. Radiat. Meas. 32, 579–583.
Ninagawa, K., Adachi, K., Uchimura, N., Yamamoto, I., Wada, T., Yamashita, Y., Takashima, I., Sekimoto, K., Hasegawa, H., 1992. Thermoluminescence dating of calcite shells in the pectinidae family. Quat. Sci. Rev. 11, 121–126.
Ninagawa, K., Matsukuma, Y., Fukuda, T., Sato, A., Hoshinoo, N., Nakagawa, M., Yamamoto, I., Wada, T., Yamashita, Y., Sekimoto, K., Komura, K., 1994. Thermoluminescence dating of a calcite shell, crassostrea-gigas (thunberg) in the ostreidae family. Quat. Sci. Rev. 13, 589–593.
Ninagawa, K., Takahashi, N., Wada, T., Yamamoto, I., Yamashita, N., Yamashita, Y., 1988. Thermo-luminescence measurements of a calcite shell for dating. Quat. Sci. Rev. 7, 367–371.
Obert, J.C., Scholz, D., Felis, T., Brocas, W.M., Jochum, K.P., Andreae, M.O., 2016. $^{230}$Th/U dating of Last Interglacial brain corals from Bonaire (southern Caribbean) using bulk and theca wall material. Geochim. Cosmochim. Acta 178, 20–40.
Ogata, M., Hasebe, N., Fujii, N., Yamakawa, M., 2017. Measuring apparent dose rate factors using beta and gamma rays, and alpha efficiency for precise thermoluminescence dating of calcite. J. Miner. Petrol. Sci. 112, 336–345.
Osmond, J.K., Cowart, J.B., Ivanovich, M., 1983. Uranium isotopic disequilibrium in ground water as an indicator of anomalies. Int. J. Appl. Radiat. Isot. 34, 283–308.
Pagonis, V., Maniatis, Y., Michael, C., Bassiakos, Y., 1997. Spurious and regenerated thermoluminescence in calcite powder samples. Radiat. Meas. 27, 37–42.
Pickering, R., Kramers, J.D., Partridge, T., Kodolanyi, J., Pettke, T., 2010. U–Pb dating of calcite–aragonite layers in speleothems from hominin sites in South Africa by MC-ICP-MS. Quat. Geochronol. 5, 544–558.
Plater, A.J., Ivanovich, M., Dugdale, R.E., 1992. Uranium series disequilibrium in river sediments and waters: the significance of anomalous activity ratios. Appl. Geochem. 7, 101–110.
Prescott, J.R., Hutton, J.T., 1994. Cosmic-ray contributions to dose-rates for luminescence and esr dating - large depths and long-term time variations. Radiat. Meas. 23, 497–500.
R Core Team, 2022. R: A Language and Environment for Statistical Computing. R Foundation for Statistical Computing, Vienna, Austria.
Rahimzadeh, N., Zhang, J., Tsukamoto, S., Long, H., 2023. Characteristics of the quartz isothermal thermoluminescence (ITL) signal from the 375 °C peak and its potential for extending the age limit of quartz dating. Radiat. Meas. 161, 106899.
Rammlmair, D., Wilke, M., Rickers, K., Schwarzer, R.A., Möller, A., Wittenberg, A., 2006. Chapter 7.6 Geology, mining, metallurgy. In: Beckhoff, B., Kanngießer, B., Langhoff, N., Wedell, R., Wolff, H. (Eds.), Handbook of Practical X-Ray Fluorescence Analysis. Springer, Berlin.
Richards, D.A., Bottrell, S.H., Cliff, R.A., Ströhle, K., Rowe, P.J., 1998. U-Pb dating of a speleothem of Quaternary age. Geochim. Cosmochim. Acta 62, 3683–3688.
Richter, M., Tsukamoto, S., Long, H., 2020. ESR dating of Chinese loess using the quartz Ti centre: a comparison with independent age control. Quat. Int. 556, 159–164.
Rogue, C., Guibert, P., Vartanian, E., Bechtel, F., Schvoerer, M., 2001. Thermoluminescence - dating of calcite: study of heated limestone fragments from Upper Paleolithic layers at Combe Sauniere, Dordogne, France. Quat. Sci. Rev. 20, 935–938.
Rusznyák, A., Akob, D.M., Nietzsche, S., Eusterhues, K., Totsche, K.U., Neu, T.R., Frosch, T., Popp, J., Keiner, R., Geletneky, J., Katzschmann, L., Schulze, E.-D., Küsel, K., 2012. Calcite biomineralization by bacterial isolates from the recently discovered pristine karstic Herrenberg cave. Appl. Environ. Microbiol. 78, 1157–1167.
Scholz, D., Hoffmann, D., 2008. 230Th/U-dating of fossil corals and speleothems. E&G Quat. Sci. J. 57, 52–76.
Sohbati, R., Murray, A., Jain, M., Buylaert, J.-P., Thomsen, K., 2011. Investigating the resetting of OSL signals in rock surfaces. Geochronometria 38, 249–258.
Spooner, N.A., 1992. Optical dating: preliminary results on the anomalous fading of luminescence from feldspars. Quat. Sci. Rev. 11, 139–145.
Spooner, N.A., 1994. The anomalous fading of infrared-stimulated luminescence from feldspars. Radiat. Meas. 23, 625–632.
Stirling, R.J., Duller, G.A.T., Roberts, H.M., 2012. Developing a single-aliquot protocol for measuring equivalent dose in biogenic carbonates. Radiat. Meas. 47, 725–731.
Tang, S.L., Li, S.H., 2015. Low temperature thermochronology using thermoluminescence signals from quartz. Radiat. Meas. 81, 92–97.
Theocaris, P.S., Liritzis, I., Galloway, R.B., 1997. Dating of two hellenic pyramids by a novel application of thermoluminescence. J. Archaeol. Sci. 24, 399–405.
Tripathi, R.M., Sahoo, S.K., Mohapatra, S., Lenka, P., Dubey, J.S., Puranik, V.D., 2013. Study of uranium isotopic composition in groundwater and deviation from secular equilibrium condition. J. Radioanal. Nucl. Chem. 295, 1195–1200.
Tsukamoto, S., Long, H., Richter, M., Li, Y., King, G.E., He, Z., Yang, L., Zhang, J., Lambert, R., 2018. Quartz natural and laboratory ESR dose response curves: a first attempt from Chinese loess. Radiat. Meas. 120, 137–142.
Tsukamoto, S., Murray, A.S., Huot, S., Watanuki, T., Denby, P.M., Bøtter-Jensen, L., 2007. Luminescence property of volcanic quartz and the use of red isothermal TL for dating tephras. Radiat. Meas. 42, 190–197.
Ugumori, T., Ikeya, M., 1980. Luminescence of $CaCO_3$ under $N_2$ laser excitation and application to archaeological dating. Jpn. J. Appl. Phys. 19, 459–465.
Vandenberghe, D.A.G., Jain, M., Murray, A.S., 2009. Equivalent dose determination using a quartz isothermal TL signal. Radiat. Meas. 44, 439–444.
Visocekas, R., 1985. Tunneling radiative recombination in labradorite - its association with anomalous fading of thermo-luminescence. Nucl. Tracks Radiat. Meas. 10, 521–529.
Wedepohl, K.H., 1995. The composition of the continental crust. Geochem. Cosmochim. Acta 59, 1217–1232.
Wigley, T.M.L., Brown, M.C., 1976. The physics of caves. The science of speleology 3 (3), 329–347.
Wintle, A.G., 1973. Anomalous fading of thermoluminescence in mineral samples. Nature 245, 143–144.
Wintle, A.G., 1974. Factors Determining the Thermoluminescence of Chronologically Significant Materials. University of Oxford. PhD thesis.
Wintle, A.G., 1975. Effects of sample preparation on the thermoluminescence characteristics of calcite. Mod. Geol. 5, 165–167.
Wintle, A.G., 1977. Thermoluminescence dating of minerals—traps for the unwary. J. Electrost. 3, 281–288.
Wintle, A.G., 1978. A thermoluminescence dating study of some Quaternary calcite: potential and problems. Can. J. Earth Sci. 15, 1977–1986.
Wintle, A.G., Murray, A.S., 2006. A review of quartz optically stimulated luminescence characteristics and their relevance in single-aliquot regeneration dating protocols. Radiat. Meas. 41, 369–391.
Woodhead, J., Hellstrom, J., Maas, R., Drysdale, R., Zanchetta, G., Devine, P., Taylor, E., 2006. U–Pb geochronology of speleothems by MC-ICPMS. Quat. Geochronol. 1, 208–221.
Woodhead, J., Petrus, J., 2019. Exploring the advantages and limitations of in situ U–Pb carbonate geochronology using speleothems. Geochronology 1, 69–84.
Wunderlich, J., Schmidt, S., Katzschmann, L., Geletneky, J., 2009. Aufwältigungs- und Befahrungsergebnisse der Herrenberg-Höhle (Höhle 1) und der Höhle 2 im Bleßberg-Tunnel - Teilbericht der TLUG. Weimar (unpublished report, available at landesgeologie@tlubn.thueringen.de).
Yang, Q., Scholz, D., Jochum, K.P., Hoffmann, D.L., Stoll, B., Weis, U., Schwager, B., Andreae, M.O., 2015. Lead isotope variability in speleothems—A promising new proxy for hydrological change? First results from a stalagmite from western Germany. Chem. Geol. 396, 143–151.
Yee, K.P., Mo, R.H., 2018. Thermoluminescence dating of stalactitic calcite from the Early Paleolithic occupation at Tongamdong site. J. Archaeol. Sci. Rep 19, 405–410.
Zhang, J., Wang, L., 2020. Thermoluminescence dating of calcite – alpha effectiveness and measurement protocols. J. Lumin. 223, 117205.
Zhang, J., Tsukamoto, S., 2022. A simplified multiple aliquot regenerative dose protocol to extend the dating limit of K-feldspar pIRIR signal. Radiat. Meas. 157, 106827.